The Abdus Salam International Centre for Theoretical Physics

United Nations Educational, Scientific and Cultural Organization
IAEA

2168-15

Joint ICTP-IAEA Workshop on Dense Magnetized Plasma and Plasma Diagnostics

15 - 26 November 2010

Quasi steady plasma accelerators

I. Garkusha
Kharkov Inst. of Physics & Technology
Kharkov
Ukraine

Quasi-Steady-State Plasma Accelerators: Physics and Applications

Presented by Igor E. Garkusha

IPP NSC KIPT, Kharkov, Ukraine

Outline

- Steady State plasma flows
- Principles of QSPA
- Experimental devices:
  QSPA Kh-50- plasma accelerator
  MPC- magnetoplasma compressor
- Dynamics of dense plasma streams generated by QSPA and MPC

- Examples of Applications
- Summary

Quasi Steady State ?

Duration of the process (discharge) essentially exceeds the time of flight of the plasma particles in the accelerating channel

$\tau/t \gg 1$ Time of flight: $t = L/v_m$

Quasi-Steady-State Plasma Flows

$$\rho\left(\frac{\partial \vec{v}}{\partial t} + (\vec{v}\nabla)\vec{v}\right) = -\nabla p + \frac{1}{c}\left[\vec{j}, \vec{H}\right] \qquad \frac{\partial \vec{H}}{\partial t} = rot\left[\vec{v}, \vec{H}\right] \qquad j = \frac{c}{4\pi} rot\vec{H}$$

$$\frac{\partial \rho}{\partial t} + div\rho\vec{v} = 0 \qquad p = p_0\left(\frac{\rho}{\rho_0}\right)^{\gamma} \qquad div\vec{H} = 0$$

In the case of stationary axial-symmetric flow: $\frac{\partial}{\partial t} = 0,\ H_r = H_z = 0,\ \upsilon_\theta = 0.$

The plasma flow is divided into flux tubes with a width h=h(z).
Under these assumptions **three conservations lows** (holding true for each flux tube) follows from above system of equations mentioned.

$$\frac{\upsilon^2}{2} + \int \frac{dp}{\rho} + \frac{H^2}{4\pi\rho} = const \equiv U$$

- Bernoulli equation
Conservation of full energy in the flow

$$i(\rho) \equiv \int \frac{dp}{\rho} = \frac{p_0}{\rho_0}\frac{\gamma}{\gamma - 1}\left(\frac{\rho}{\rho_0}\right)^{\gamma-1}$$

$$\frac{H}{\rho r} = const \equiv æ$$

- Freezing-in azimuth magnetic flux into plasma

$$\rho\upsilon r f = const \equiv \dot{m}$$

- Mass conservation law

For z=0 and $\upsilon \to 0$ one possible to find **the CONSTANT of Bernoulli**

$$U \equiv \frac{H_0^2}{4\pi\rho_0}(1+\mu),$$

$$Here: \ \mu \equiv \frac{i_0}{c_{A0}^2}, \quad c_A^2 = \frac{H^2}{4\pi\rho} - Alfven \ \ velocity$$

MHD analog of Laval nozzle

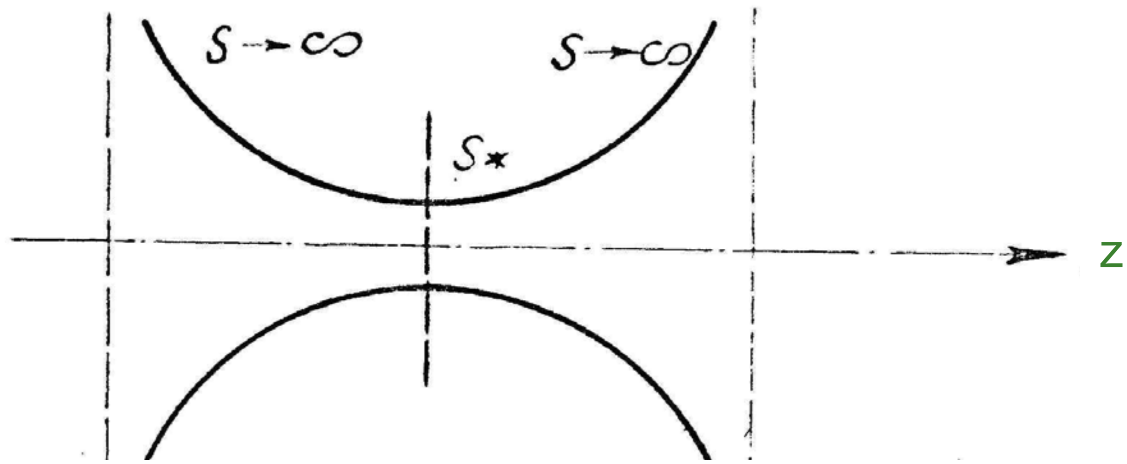

$$S = \frac{\dot{m}}{\rho v}$$

$$\rho \to \rho_0, v \to 0$$

$$\rho \to 0, v \to v_{\max}$$

Minimal cross section,

Subsonic and supersonic flows

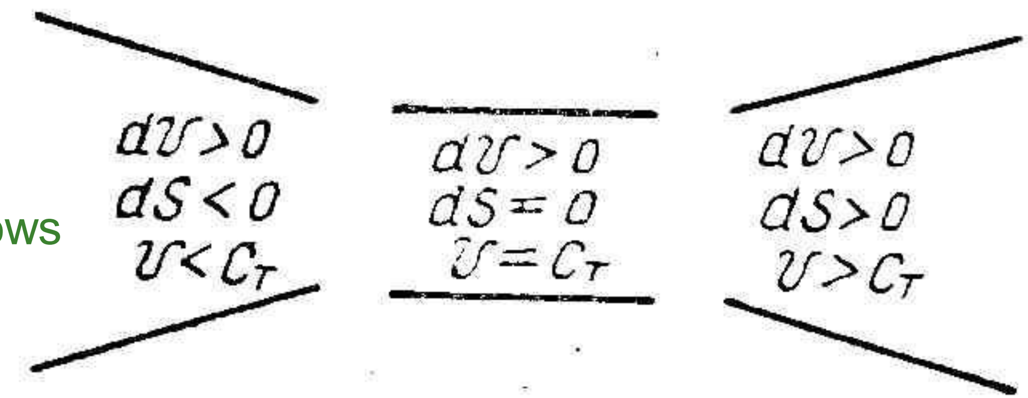

$$i(\rho_0) << \frac{H_0^2}{4\pi\rho_0}$$

$$\frac{\upsilon^2}{2} + \frac{H^2}{4\pi\rho} = \frac{H_0{}^2}{4\pi\rho_0} \qquad \frac{\upsilon^2}{2} + \frac{H_0^2}{4\pi\rho_0}\frac{\rho}{\rho_0} = \frac{H_0{}^2}{4\pi\rho_0}$$

$$\rho \to 0$$

For $\mu << 1$ at z = 0 al flow energy is concentrated in the magnetic field.
In the process of plasma flow, for Z > 0, one possible to have **two extreme cases:**

$$\frac{H^2}{4\pi\rho} \to \frac{\upsilon^2}{2}$$

- Purely **accelerating regime** with maximum velocity:

$$\boldsymbol{v_{max} = (2)^{1/2} v_{A0} = H_0/(2\pi\rho)^{1/2}}$$

$$\frac{H^2}{4\pi\rho} \to i(\rho)$$

- Purely **compression regime** with

$$i(\rho_{\max}) = U = C_{A0}^2 \qquad \frac{\rho_{\max}}{\rho_0} = \left[(\gamma - 1)\frac{c_{AO}^2}{c_{TO}^2}(1+\mu)\right]^{\frac{1}{\gamma-1}}$$

Here $c_{TO} = \sqrt{\gamma \frac{p_0}{\rho_0}}$ is sound velocity,

γ - ratio of specific heats

(For adiabatic compression of hydrogen ($\gamma = 5/3$) $c_{A0} = 10^8$ cm/s, $c_{T0} = 10^6$ cm/s the maximum value of compression is of an order 5.10^5).

$$div\, n\vec{v}_i = 0, \quad div\, n\vec{v}_e = 0$$ а)

$$M\frac{d\vec{v}_i}{dt} = -\nabla\varphi + \frac{1}{c}\left[\vec{v}_i, \vec{H}\right] - \cancel{\frac{\nabla p_i}{en}}$$ б)

$$0 = -\nabla\varphi + \cancel{\frac{\nabla p_e}{en}} + \frac{1}{c}\left[\vec{v}_e, \vec{H}\right];$$

$$p_e = p_e(n); \quad p_i = p_i(n),$$ в)

$$rot\vec{H} = \frac{4\pi}{c} en(\vec{v}_i - \vec{v}_e).$$ г)

$$\frac{\partial}{\partial r} rnv_r^{i,e} + \frac{\partial}{\partial z} rnv_z^{i,e} = 0$$

$\Psi_{i,e}$ - flux functions of ions and electrons

$$rn\upsilon_z = \frac{\partial\psi}{\partial r}; \qquad rn\upsilon_r = -\frac{\partial\psi}{\partial z}$$

$\Rightarrow$ Ion and Electron Trajectories equations

$\Psi i\ (r,z)$ = const; $\Psi e\ (r,z)$ = const.

$$\mathbf{E} + \frac{\vec{v}_e}{c} \times \mathbf{H} = 0$$

Ev_e = 0, electrons move along equipotential lines

$$\frac{M\upsilon_i^2}{2} + e\varphi = U_i(\psi_i)$$

$\varphi = \varphi\ (\Psi_e)$

$-e\varphi = U_e\ (\Psi_e)$

Analogy with drift approximation

$$\frac{d\vec{R}}{dt} = v_{II}\frac{\vec{H}}{|H|} + \vec{U}_E + \frac{Mc}{e}\left[\frac{d\vec{U}_E}{dt}, \vec{H}\right]\frac{1}{H^2}$$

$$\vec{U}_E = \frac{c\left[\vec{E}, \vec{H}\right]}{H^2} \qquad U_E = c\frac{E}{H}$$

Simplified QSPA (with solid electrodes)

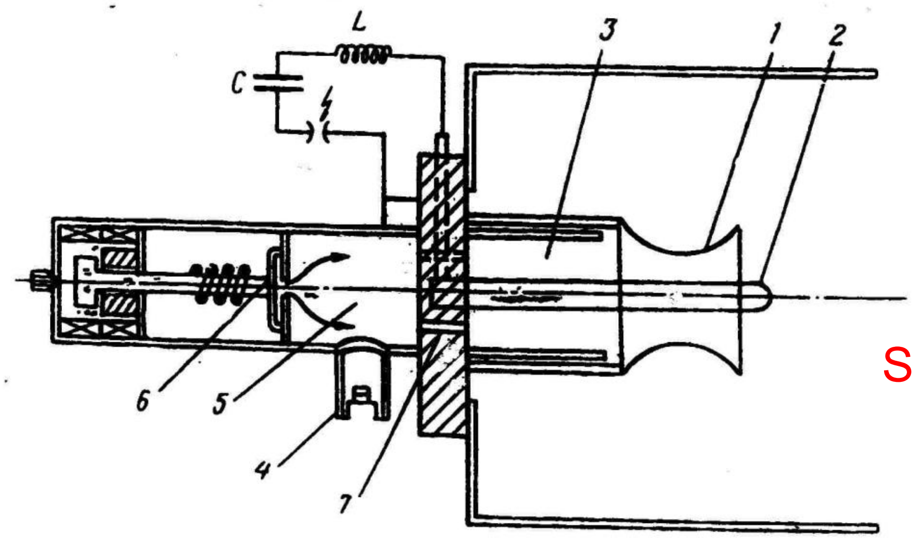

Sub-critical and post-critical regimes
CVC
Crisis of current

Experiments in simplified QSPA with non-transparent coaxial electrodes, revealed some undesirable effects

- “anode current creep”),
- instability of the ionization zone,
- high erosion of electrodes (cathode potential jump) etc.,

resulted in disturbance of the accelerating process. All these effects, restricting the plasma parameters to be achieved, were avoided in two-stage accelerator with semi-transparent active or passive electrodes-transformers. One of the most powerful such a full-block QSPA (QSPA Kh-50) was installed in the IPP NSC KIPT.

Full Block Quasi-Steady-State Plasma Accelerator QSPA Kh-50

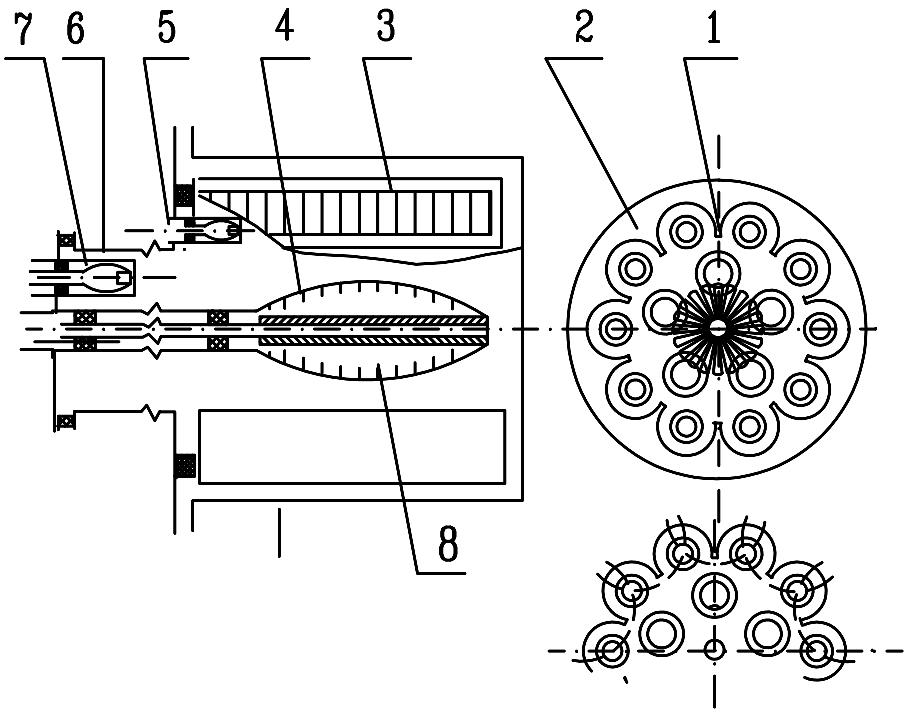

The block diagram of the QSPA Kh-50

1- anode transformer;
2- anode collector;
3- anode wafers;
4- cathode transformer;
5- anode ionization chambers (AIC);
6- drift channel;
7- input ionization chambers (IIC);
8- needle-shaped cathode emitters.

The full-block powerful quasi-steady-state plasma accelerator consists of two stages. The first one is for plasma production and pre-acceleration. The second stage (main accelerating channel) is a coaxial system of shaped active electrodes-transformers with magnetically screened elements (those elements are current supplied either from independent power sources or branching partly the discharge current in self-consistent regime of operation).

The discharge current between the electrodes-transformers is carried by ions (!).

QSPA Kh-50 Device

Maximal energy of capacitors supplying the main discharge WC is 2.25 MJ (plus 2 MJ for auxiliary systems). Main results were obtained with capacitor voltage of the main discharge up to 15 kV (W ≈ 0.8 MJ). The maximum discharge voltage achieved 12 kV and maximum discharge current - 750 kA.

Plasma Streams Magnetization

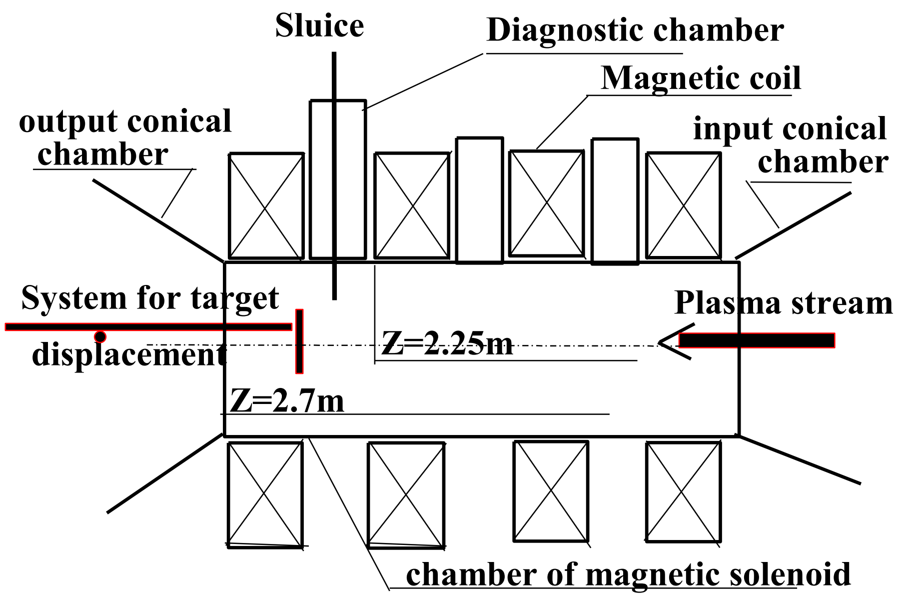

Radial dependencies of the magnetic field in plasma, normalized to vacuum magnetic field.

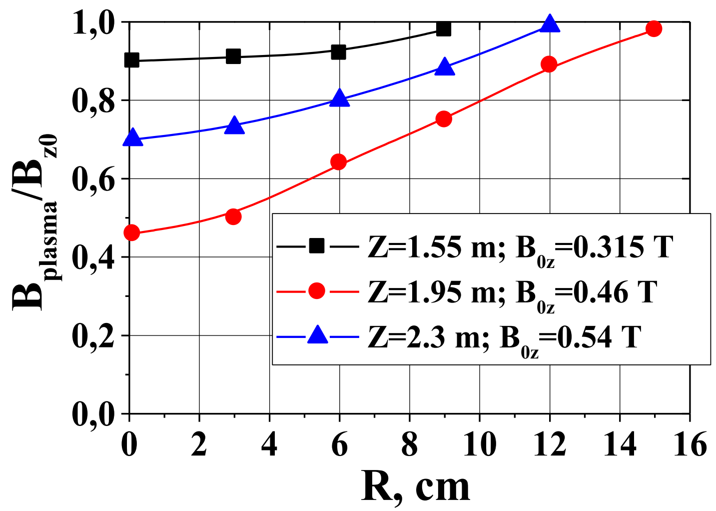

MPC device (magnetoplasma compressor)

U_c = 25-30 kV C = 90 μF

τ= 5-20 μs C_{valve} = 700 μF, U_v= 3 ÷ 5 kV

$\varnothing_c$=6cm, 3 cm

$\varnothing_a$=11 cm, 8 cm

Xenon, Helium +Xenon (independent injections),

nitrogen, argon, krypton ….

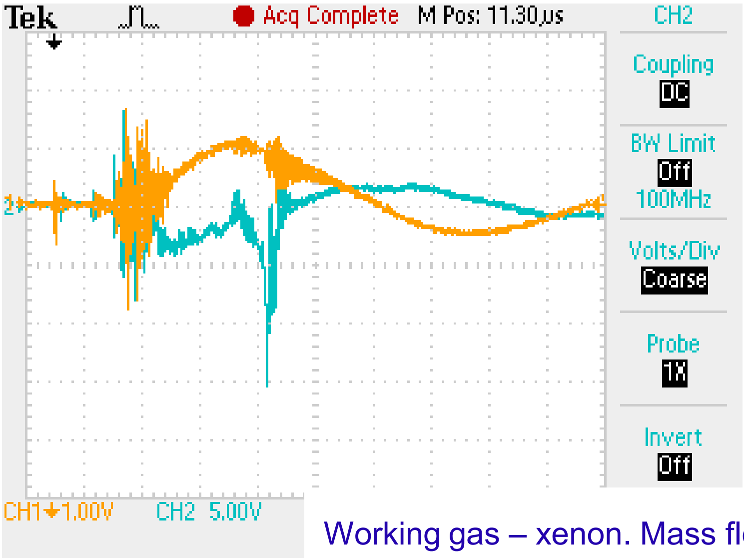

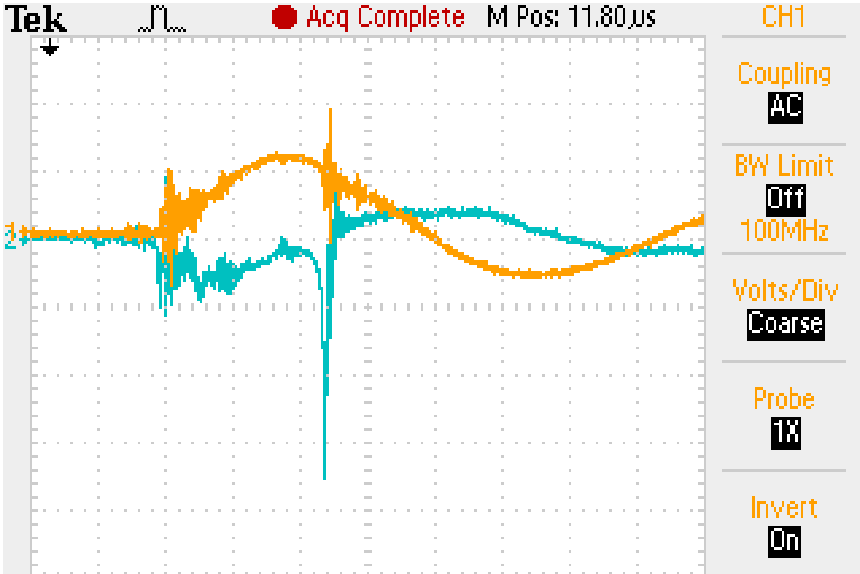

Working gas – xenon. Mass flow rate 10 cm^3. Capacitor voltage 20 kV. Time delay 500 and 550 μs.

General view of MPC device

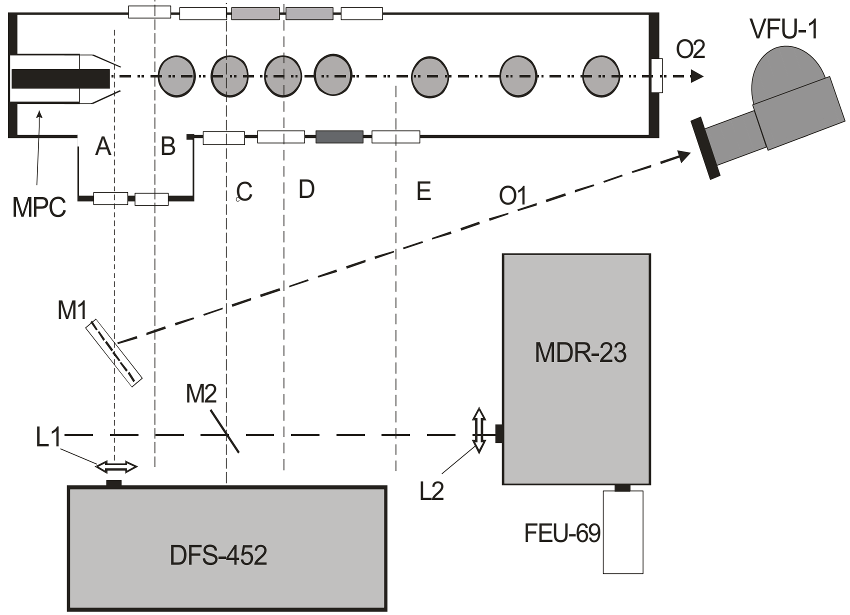

L1, L2 – condensers, M1, M2 optical mirrors.
A(1.5 cm), B(5 cm), C(20cm), D(40cm), E(80 cm) diagnostics cross-sections at the corresponding distances from MPC output.

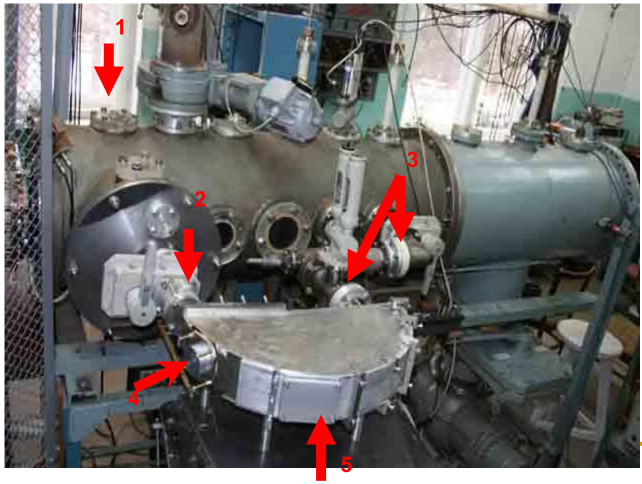

EUV spectrometer

1 – UV, EUV, X-ray source, 2 – valve and entrance slit, 3 – vacuum line to turbo-molecular pump, 4 – mount for crystal/grating, 5 – mount for detector (MCP, film).

Dynamics of discharge in QSPA

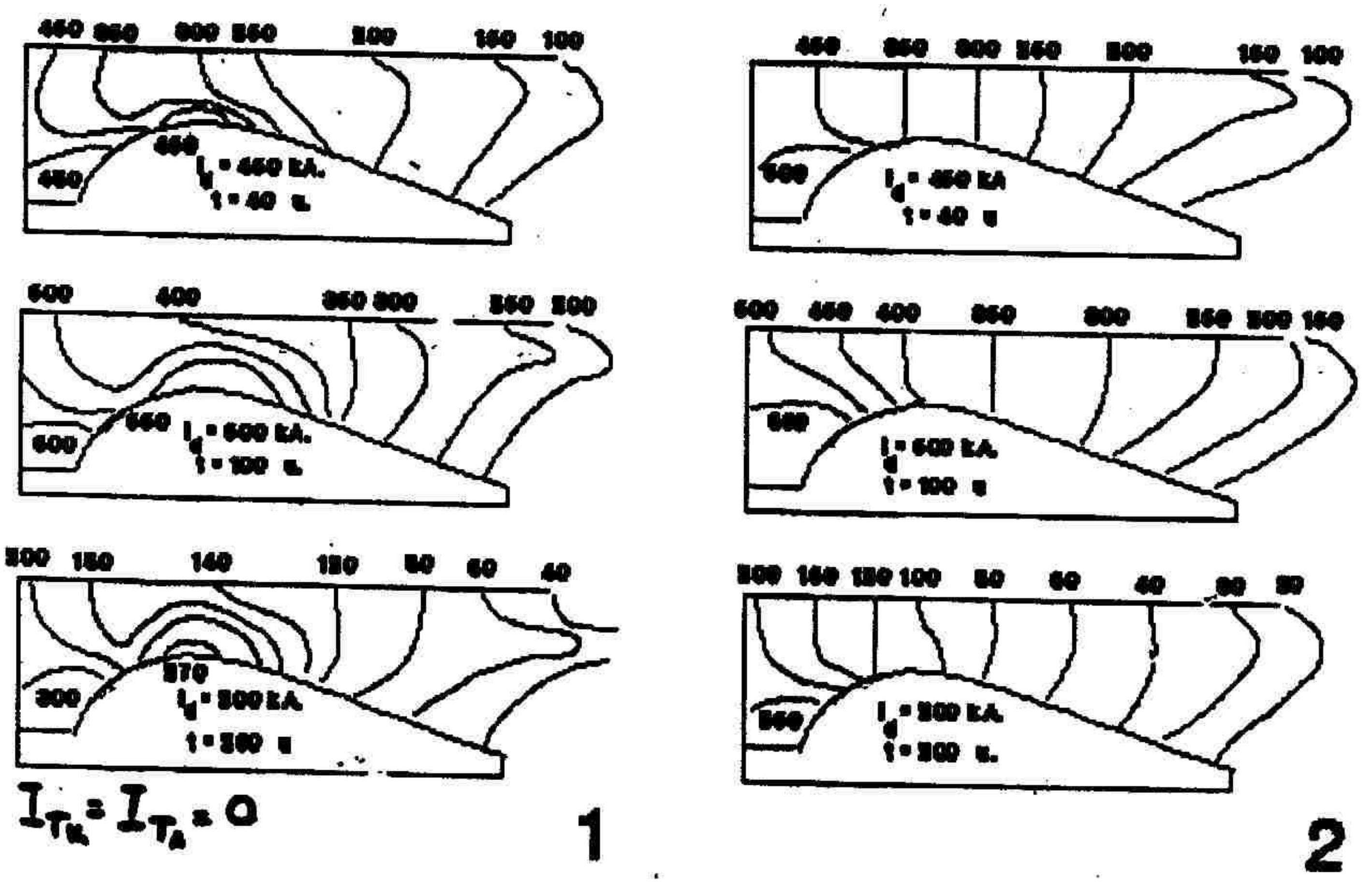

Distributions of discharge current in different operation modes

Time dependence of plasma velocity

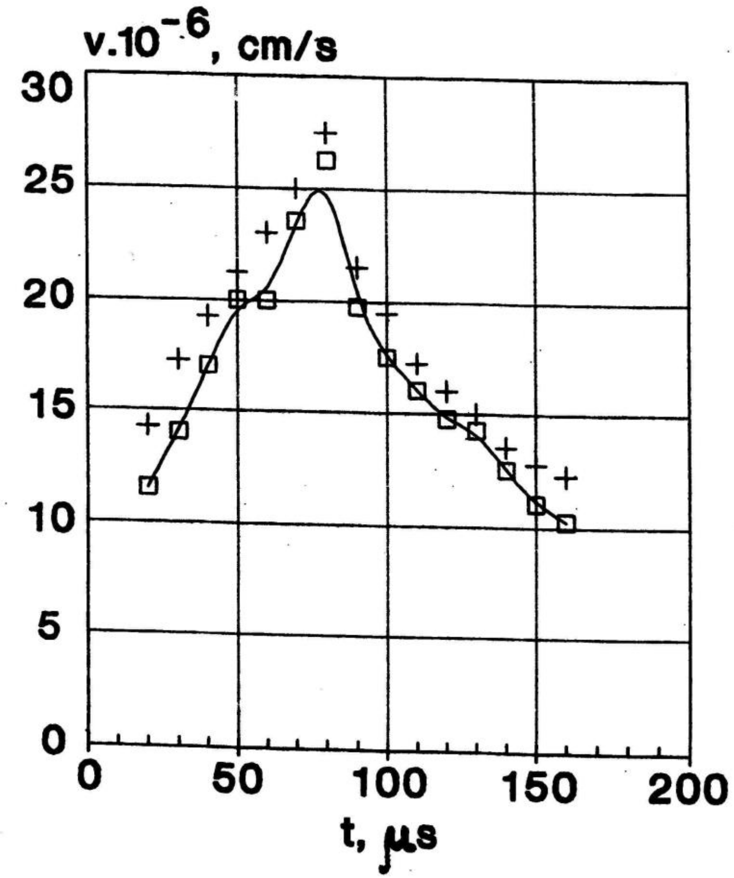

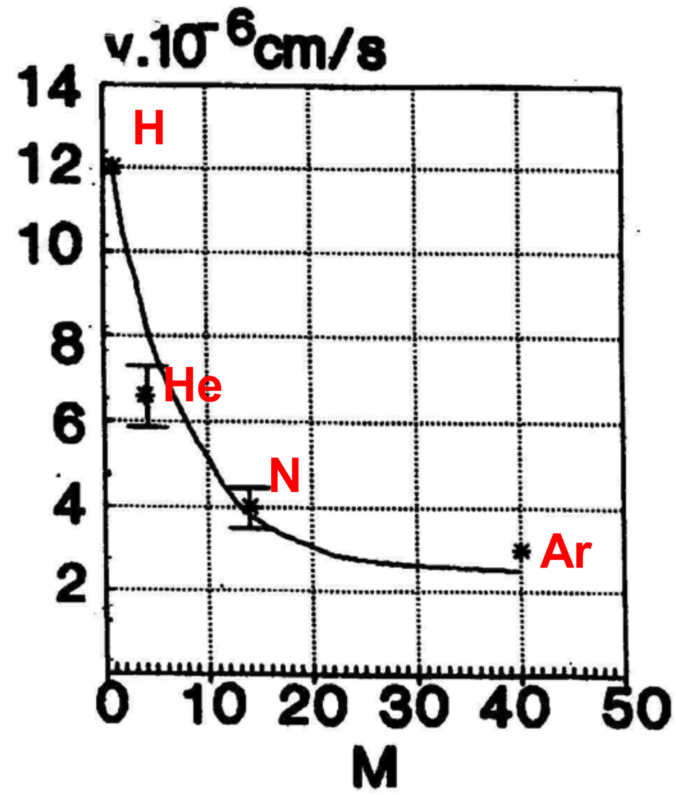

Plasma velocity versus mass of gas ions

□ - experiment

+ - $v_{max} = (2)^{1/2} v_{A0} = H_0/(2\pi\rho)^{1/2}$

Theoretical dependencies between plasma and electrotechnical parameters of the QSPA:

$$v = \vartheta \cdot \left(\frac{e}{M}\right) \cdot \frac{I_d^2}{I_{\dot m}} \qquad U_d = \left(\frac{\vartheta^2}{2\eta}\right) \cdot \left(\frac{e}{M}\right) \cdot \frac{I_d^3}{I_{\dot m}}$$

Experimental dependencies on current discharge

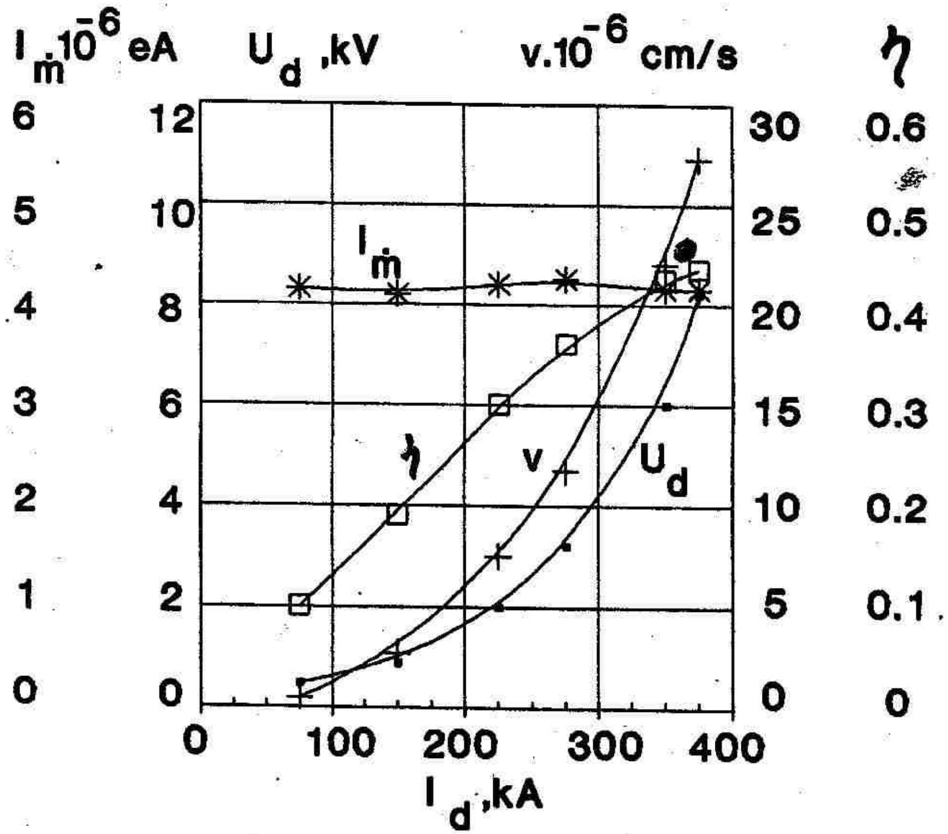

Here:
v – plasma velocity;
e – electron charge;
M – mass of ion;
η - coefficient of efficiency;
I_d *- discharge current;*
$I_{\dot m}$ *- mass consumption (in current units);*
θ *- geometrical factor.*

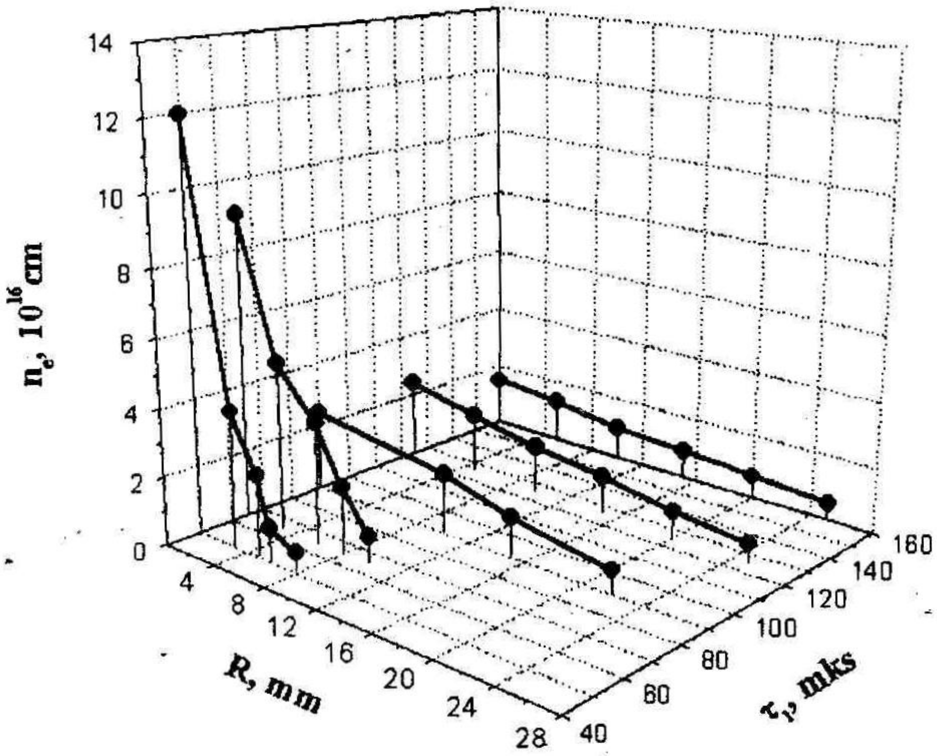

Fig. 3. Time variation of compression region density profiles: 1 - τ = 50 μs; 2 - τ = 65 μs; 3 - τ = 90 μs; 4 - τ = 120 μs. : 5 - τ = 160 μs.

Two-gases scenario of operation MPC

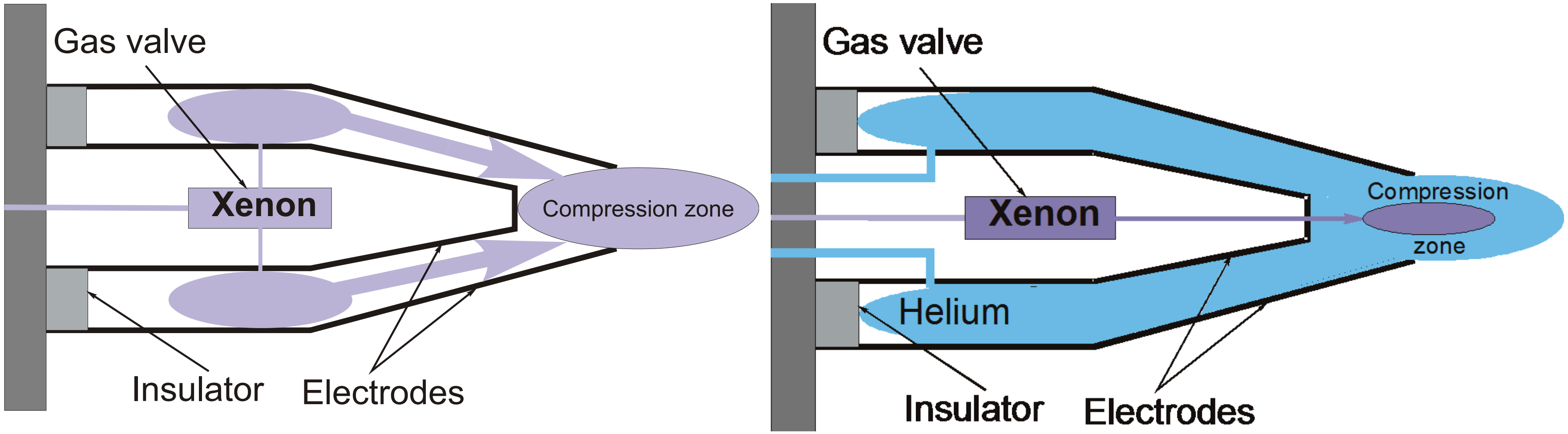

! Disadvantage ! - resonant absorption of EUV radiation from axis region by periphery xenon plasma or/and neutrals

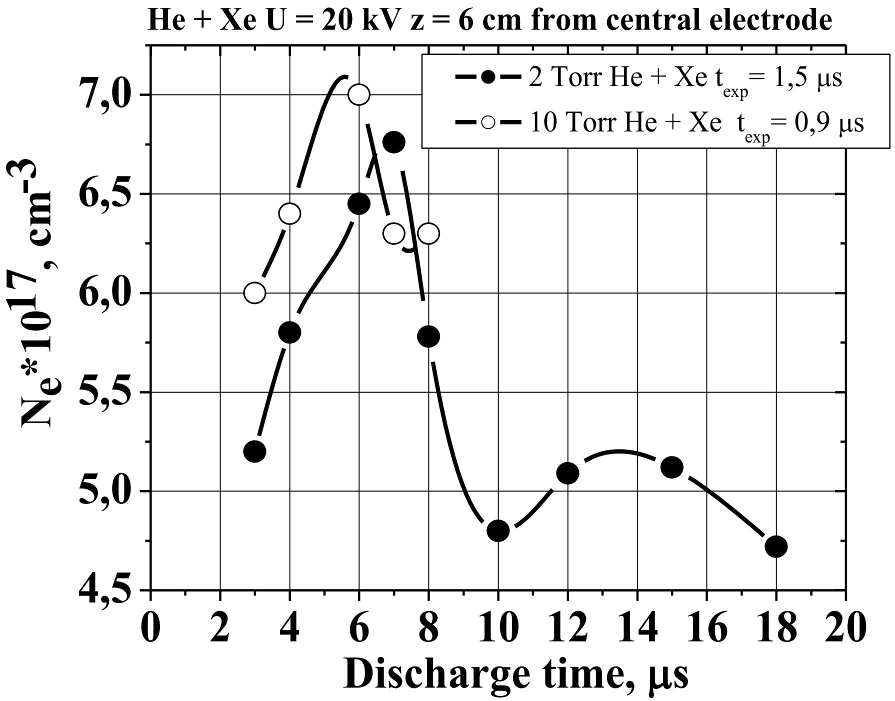

Temporal evolution of chord averaged N_e for different MPC operation regimes.

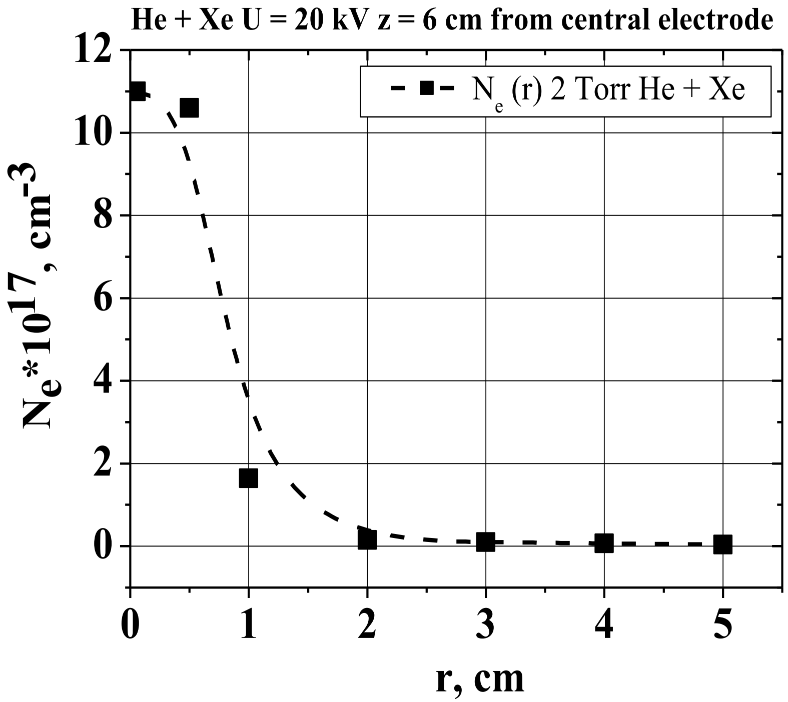

Radial distribution of the Ne at 6 µs after discharge beginning.

Dynamics of Xe plasma streams in MPC device

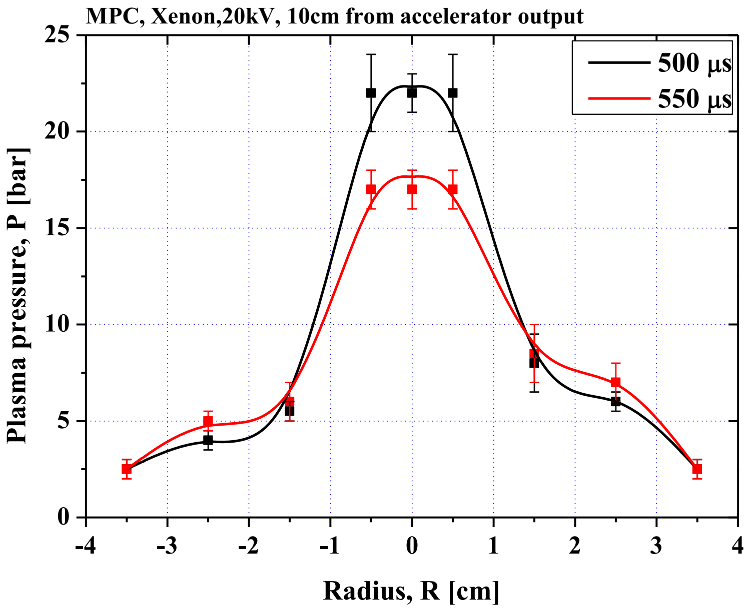

Radial distributions of plasma pressure

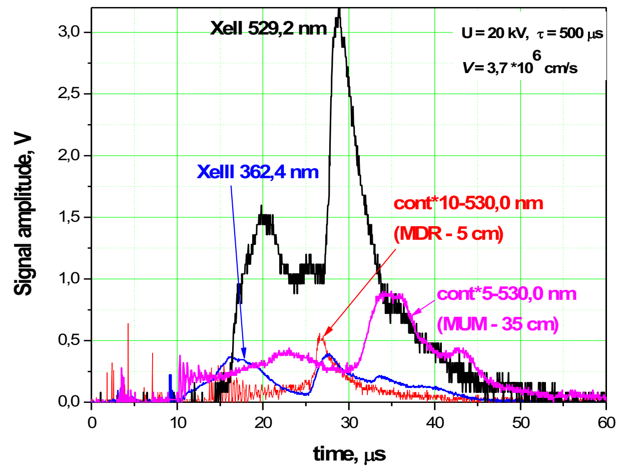

Time dependence of Xe lines and continuum luminosity in visible wave range

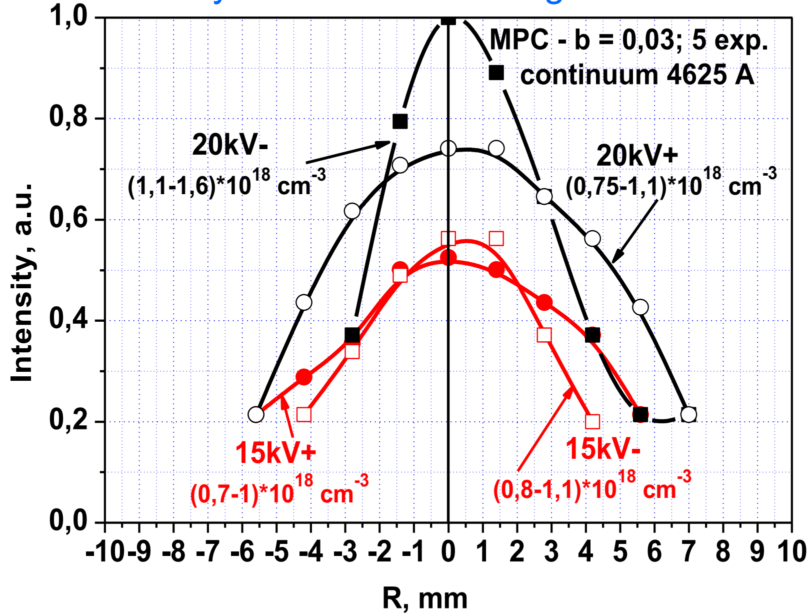

Radial distributions of continuum intensity in compression region

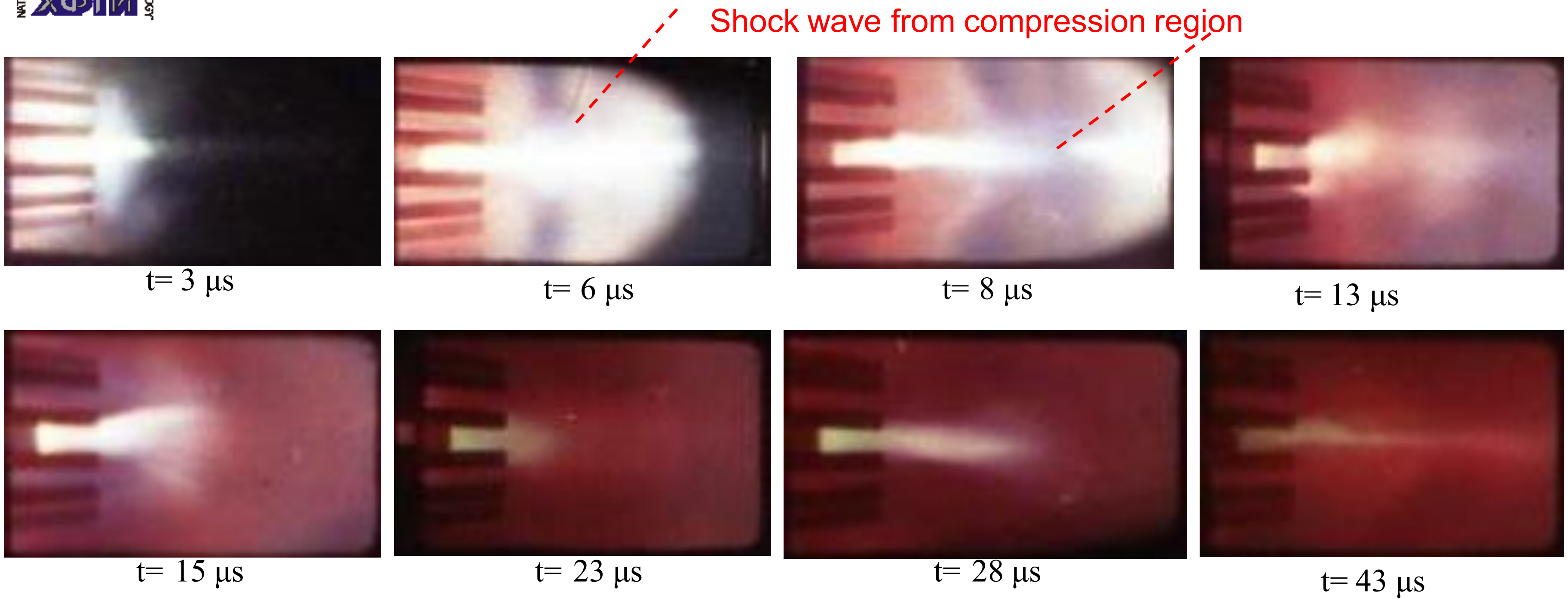

High-speed imaging of plasma compression with exposition of 1 μs

$(2\text{-}4).10^6$ cm/s

Output currents dynamics

P(helium) = 2 Torr

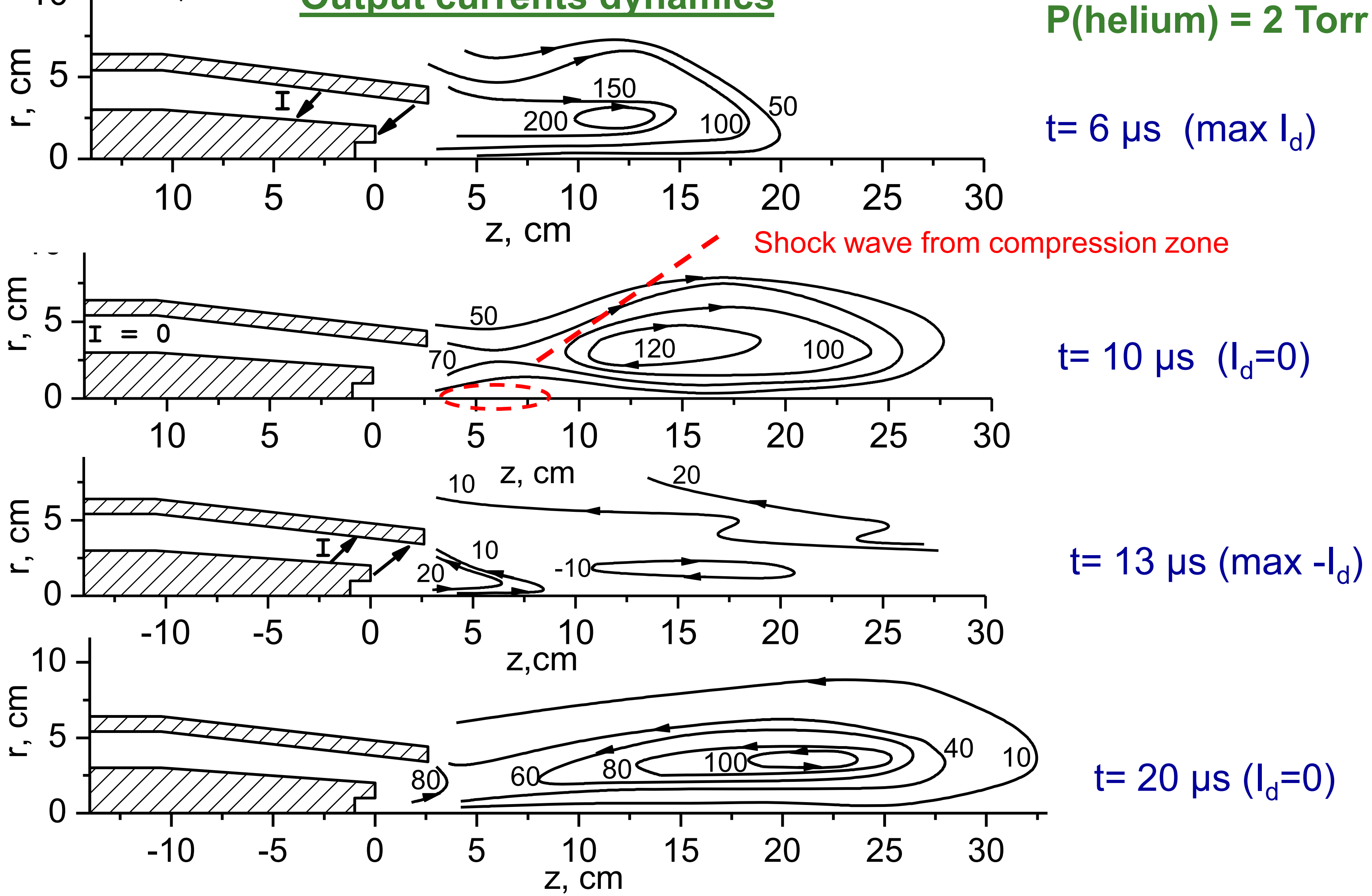

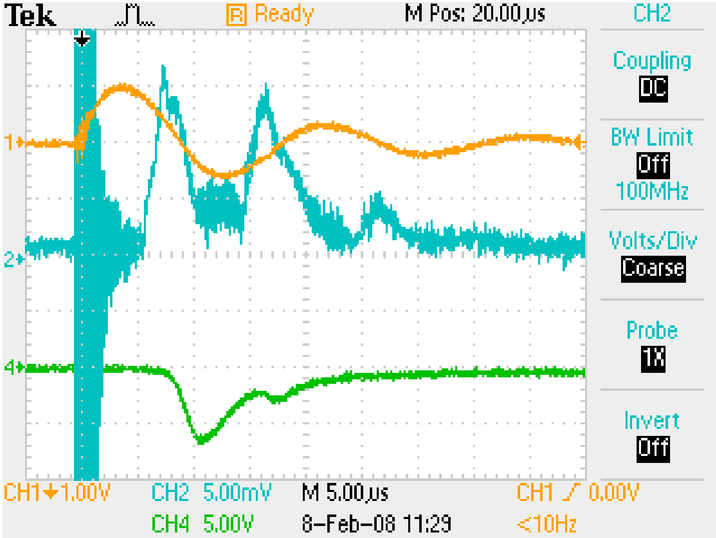

1 - Wave forms of discharge current,

2 - AXUV signal for 12.2-15.8 nm

4 - signal from photodiode in visible wave length range for local Xe injection. Discharge current in maximum is 400 kA.

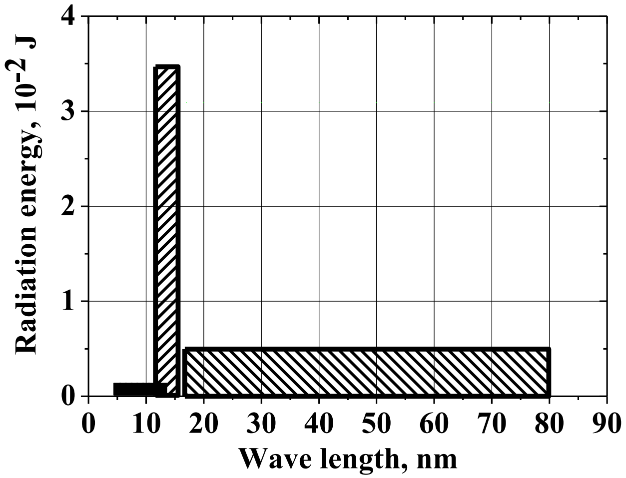

Radiation energy in different spectrum region at time delay 460 µs. Maximum discharge current 400 kA (Uc= 20 kV), Xenon gas pulse supply DV=10 cm3

$Q=(0.8\text{-}1)10^{-1}$ J $\quad P_{peak}$ =15-18 kW

Characterization of plasma streams generated by MPC device

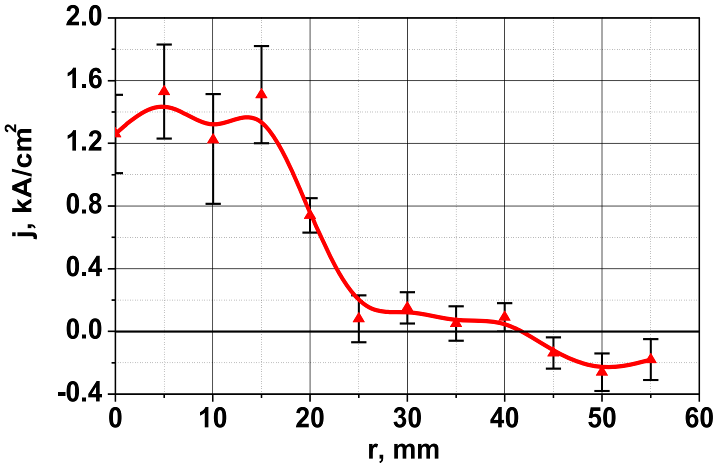

Radial distribution of electrical current density in plasma stream. Capacitor bank voltage 15 kV.

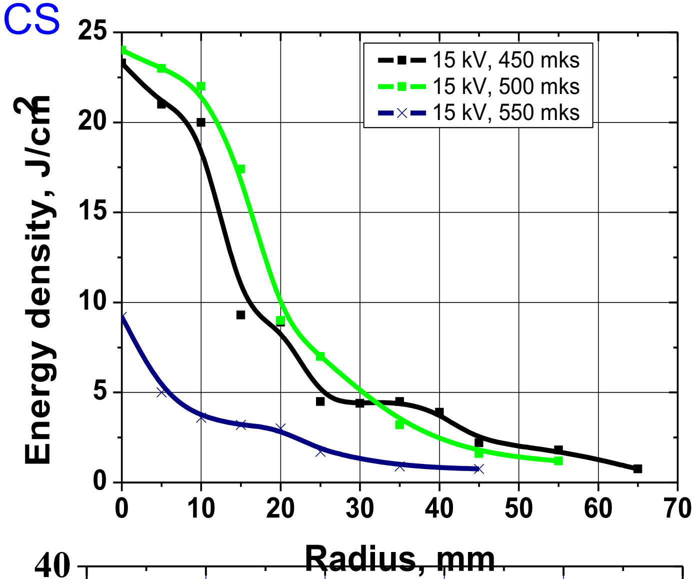

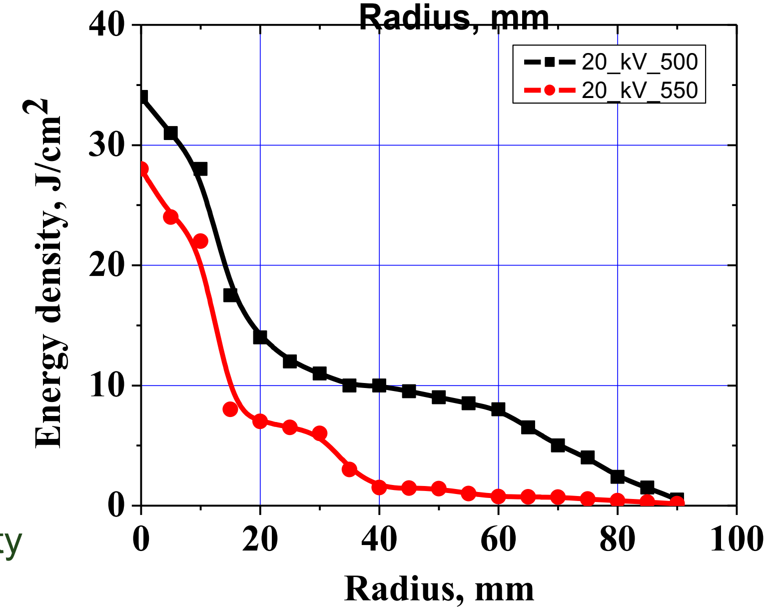

Radial distributions of energy density in xenon plasma stream.

Some applications

Investigations of dense magnetized plasmas of different gases are in importance for various scientific and technological applications:

- ✓ **the generators of hot plasma and efficient fuelling techniques (plasmoids),**
- ✓ **testing of fusion reactor materials with high energy loads,**
- ✓ **Surface modification and improvement of material properties**
- ✓ **application of dense plasma as the source of ions and radiation in different wave length ranges.**

In particular, dense xenon plasma cloud can provide effective shielding of divertor plates and mitigation of disruptions due to high emissivity of xenon and resulting re-radiation of impacting energy.

Next step lithography 13.5 nm. Laser produced and gas discharge plasma.

PSI Issues in Fusion Reactor ITER

Experimental simulation of conditions at the divertor plates.

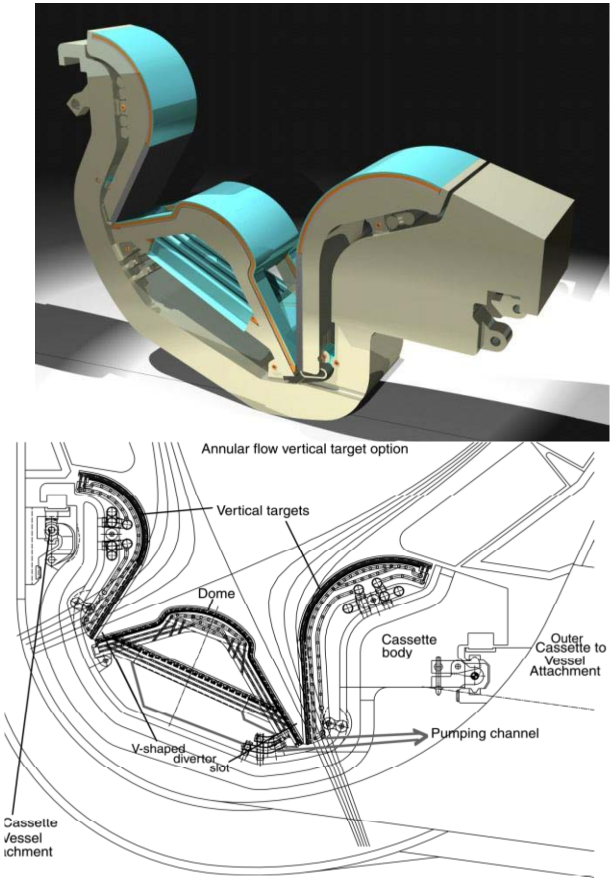

Cassette of ITER divertor

QSPA Kh-50 is unique device for simulations of conditions at the divertor plates of fusion reactor ITER under transient events.

Expected parameters of heat fluxes to the divertor plates:

Current disruption:

$Q = (10\text{-}100)\ MJ/m^2$;
$t = (1\text{-}10)$ мс

Edge Localized Modes (ELMs):

$Q = (1\text{-}3)\ MJ/m^2$;
$t = (0.1\text{-}0.5)\ ms$;
$\nu = (1\text{-}10)\ Hz$

Plasma Parameters in Different Working Regimes

Disruption simulation Regime:

- ✓Vapor shielding
- ✓Melt velocities expected for ITER disruptions (P=2-7 bar, t=1-10 ms)

ELM simulation:

- ✓ Lower energy and pressure

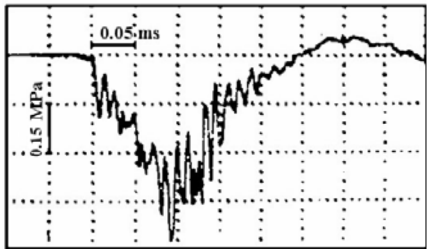

Plasma pressure signal in ELM regime1

Parameters	Disruption simulation regime	ELM simulation no melting	ELM simulation melting	ELM simulation evaporation
Plasma stream energy density [MJ/m^2]	25-30	0.9-1.0	1.2-1.5	2.4-2.5
Target Heat Load [MJ/m^2]	0.65-0.7	0.45	0.7-0.75	1-1.1
Plasma load duration [ms]	~0.25	0.25	0.25	
Half-height width [ms]	0.1-0.14	0.1-0.12	0.17	0.1-0.14
Shape of heat signal	triangular	triangular	bell	triangular
Maximal plasma pressure [bar]	16-18	4.8	3.2	4.5
Average plasma density [10^{16} cm^{-3}]	4-8	1.5-2.5	0.5-0.7	0.2-0.3
Plasma stream diameter [cm]	10-12	12-14	18	16
Number of pulses		250	450	250

Vapor shield effects

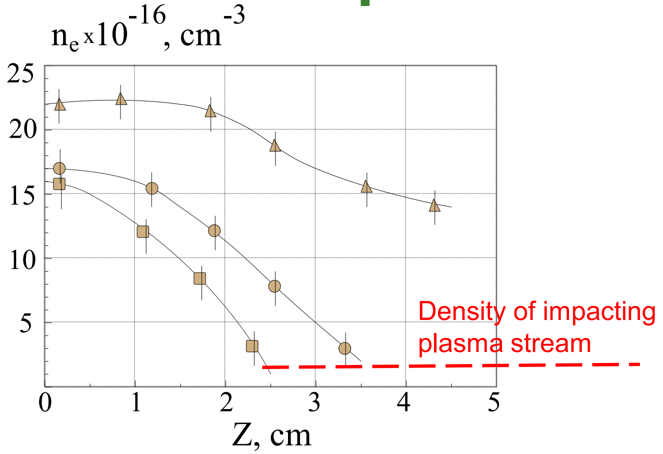

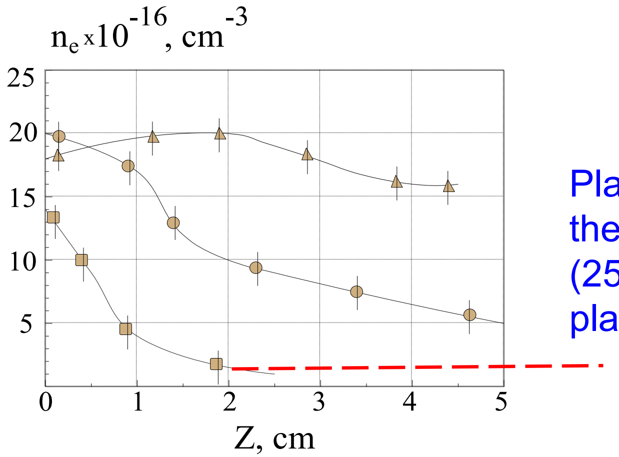

■ – B_{z0}= 0; ● – B_{z0}= 0.36 T; ▲ – B_{z0}= 0.72 T, target diameter 8 cm).

Plasma density vs. the distance from the target surface.
(25 MJ/m^2, $\Delta\tau$=20 μs and 200 μs from the beginning of plasma interaction with the surface).

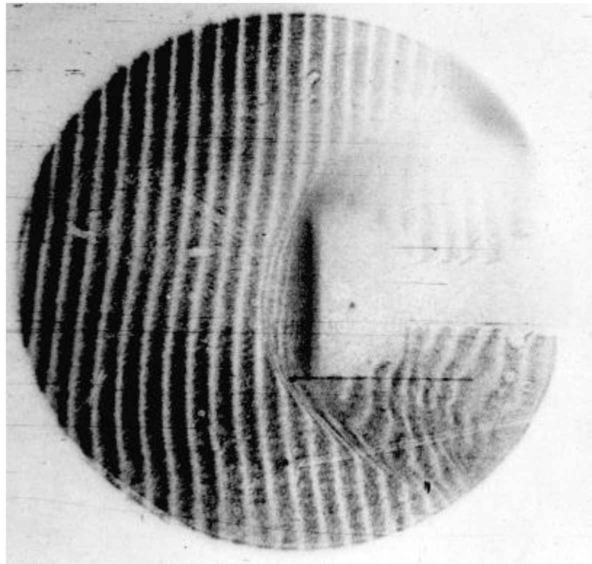

Interferometric picture of plasma interaction with graphite surface

The thickness of shielding layer grows with increasing magnetic field value and time delay of measurements with respect to the beginning of plasma interaction with a target.

Plasma shield formation in front of the graphite target in disruption simulation experiments

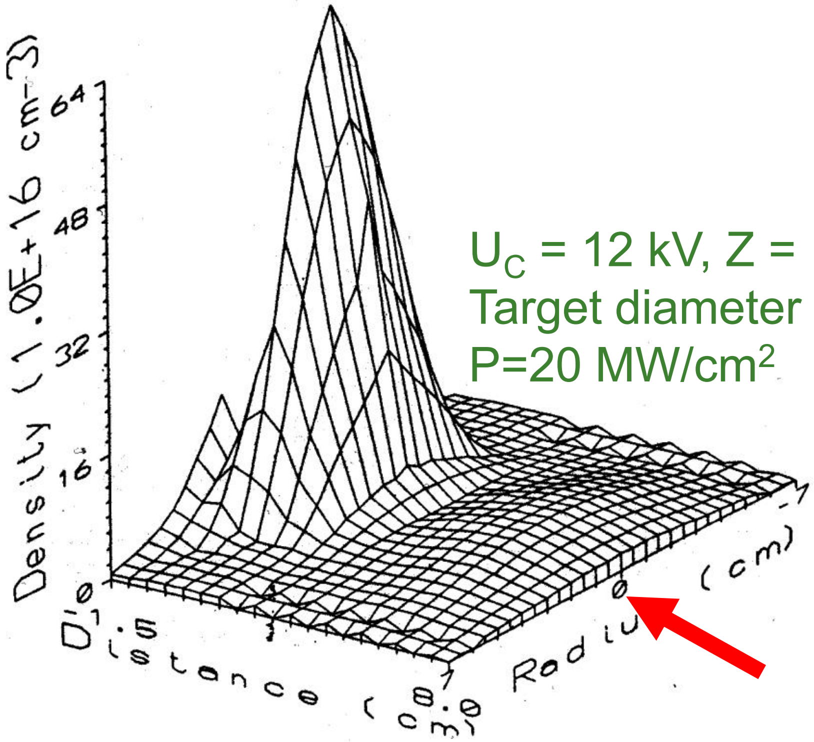

U_C = 12 kV, Z = 1.5 m,
Target diameter – 8 cm,
P=20 MW/cm²

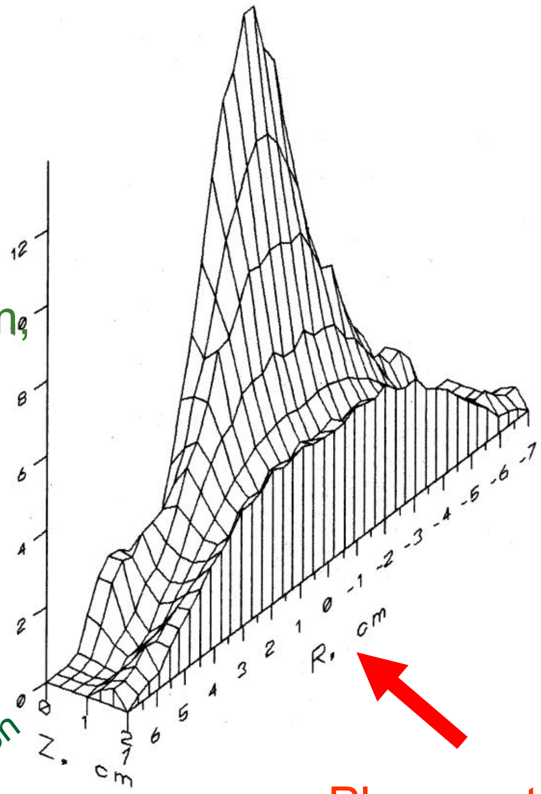

Z=0 target position

Plasma stream

Distributions of electron density obtained from interferometry

Distributions of plasma density in front of the graphite surface

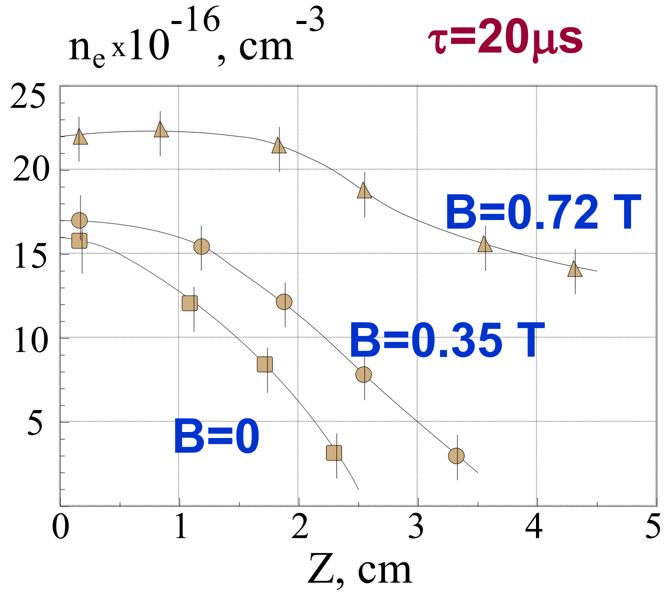

Chord averaged density vs. the distance from C-target

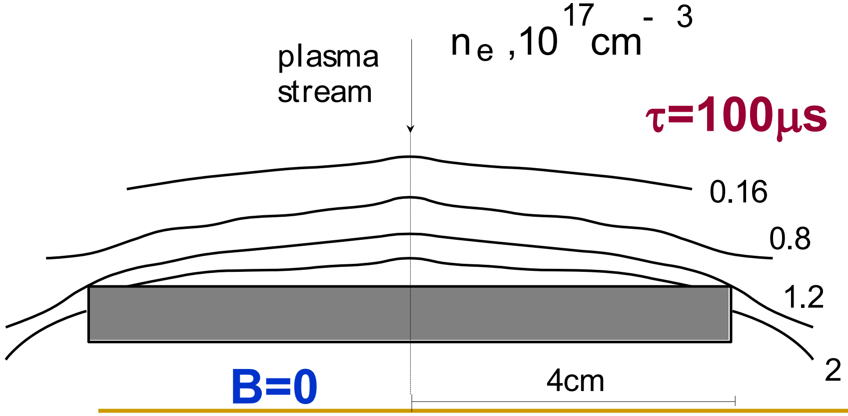

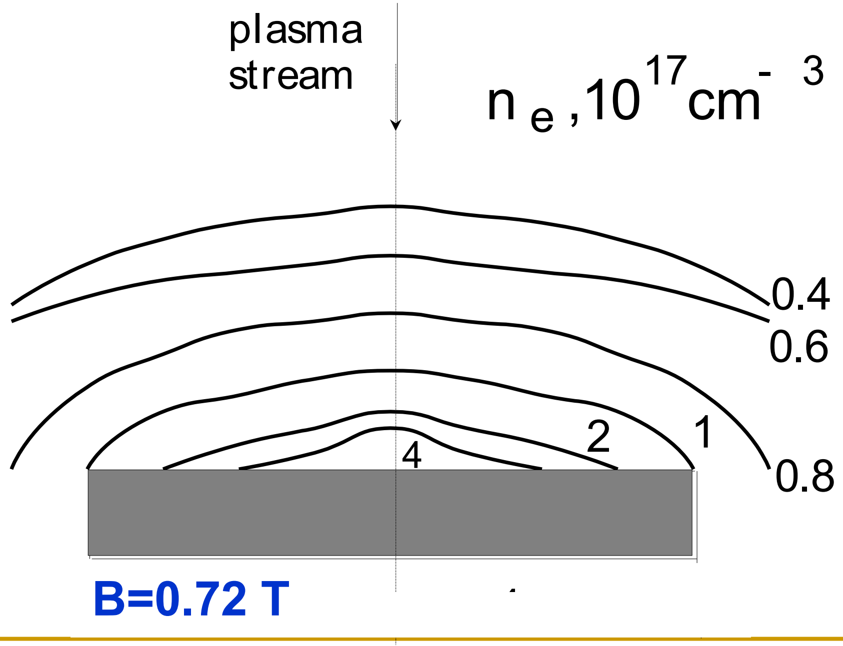

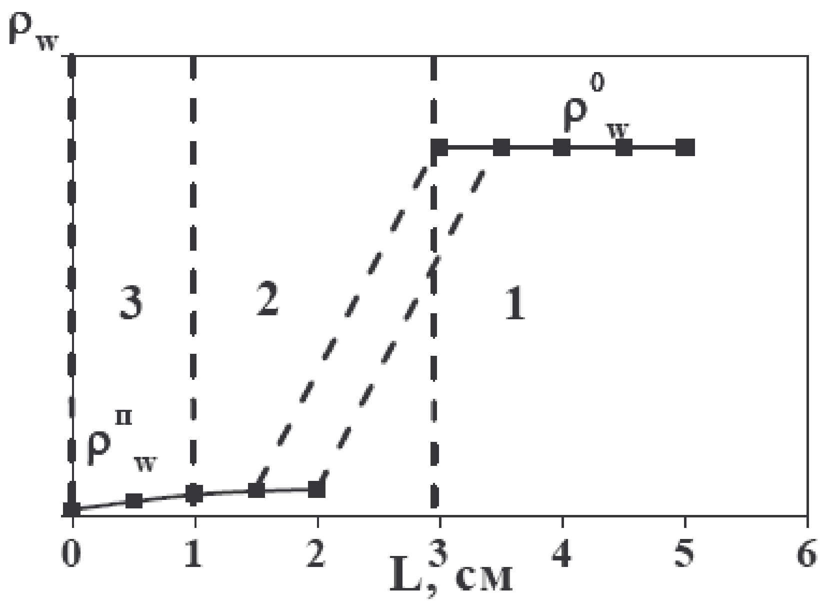

Energy density in the intermediate plasma layer versus the distance (L) from the target.
ρ^0_W – energy density in the incident plasma; ρ^s_W – energy density in the near-surface layer.
1 – incident plasma stream; 2 – region of the main energy dissipation; near-surface region.

Radiation from plasma shield

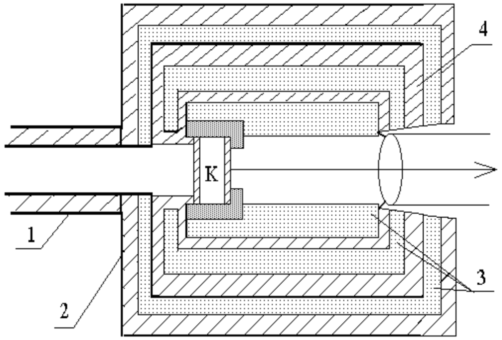

Pyroelectric detector

$\lambda \leq 3000$ Å

$\lambda < 1100$ Å

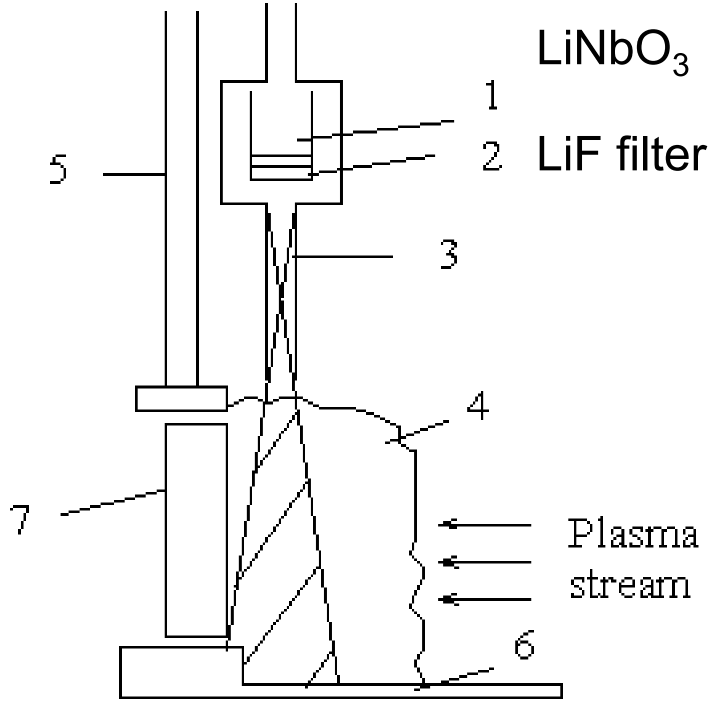

1-detector, 2-filter, 3-diaphragms, 4-shielding layer, 5-holder, 6- restrictor, 7-target

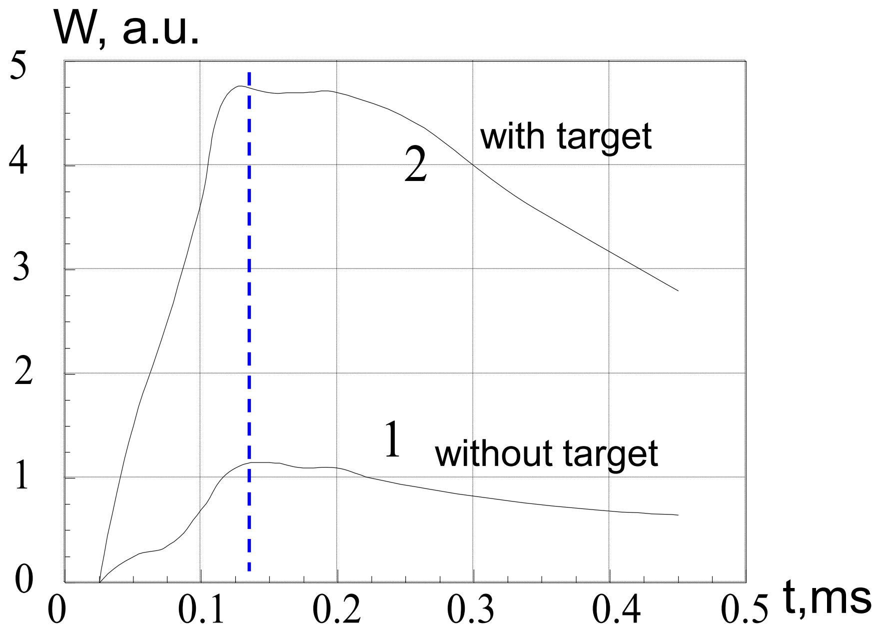

Due to the shield, the intensity of radiation is increased in 10 times. Maximal radiation is from periphery of plasma shield (1-2 cm from the surface). Thickness of periphery layer ~ 5 mm.

Influence of target atomic mass on shield dynamics

Target materials: Tungsten, Copper, Titanium, Aluminum, Graphite, Fluoroplastic F_4C

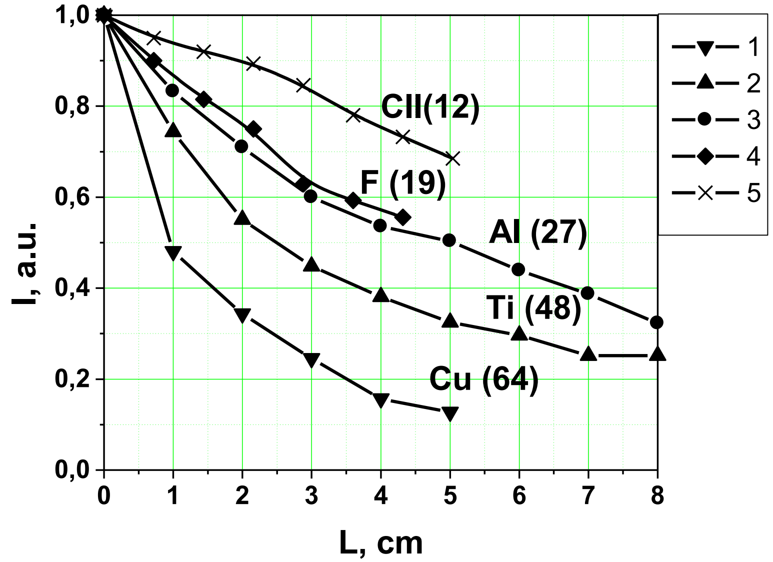

Spatial distributions of evaporated material in front of the surface for different exposed targets. (Results evaluated from spectral lines: CuII (2590Å), TiII (4534Å), AlII (5593Å), FII (4109Å) and CII (4267Å))

The evaporated material with higher atomic weight value became more "pressed" to the target surface due to the lower thermal velocities and diffusion coefficient.

Despite of an intense surface melting of tungsten it was impossible to draw it distribution in the vapor shield.

The tungsten vapor is concentrated just in front of the target and the shield thickness in this case is comparable with spatial resolution of applied spectroscopic measurements.

V.Tereshin et al. Plasma Phys. Contr.Fus.2007

Tungsten Exposure with Surface Heat Loads Close to Evaporation Threshold

Plasma Stream energy density

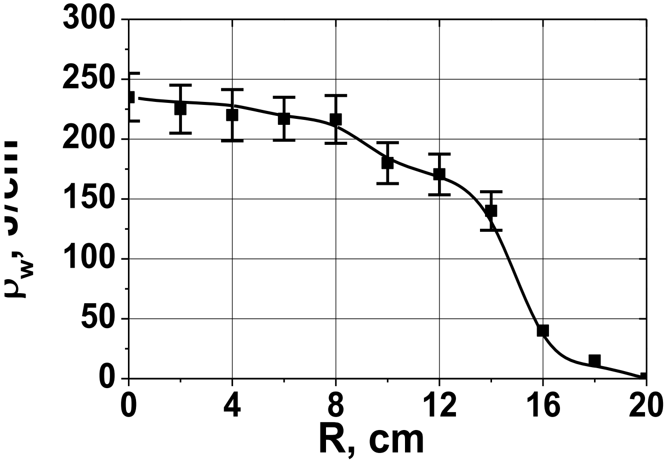

High-speed photography of tungsten evaporation

Surface load -1.1 MJ/m^2

rather thin layer < 0.5 cm
large atomic mass of tungsten
movement of evaporated W
around the target

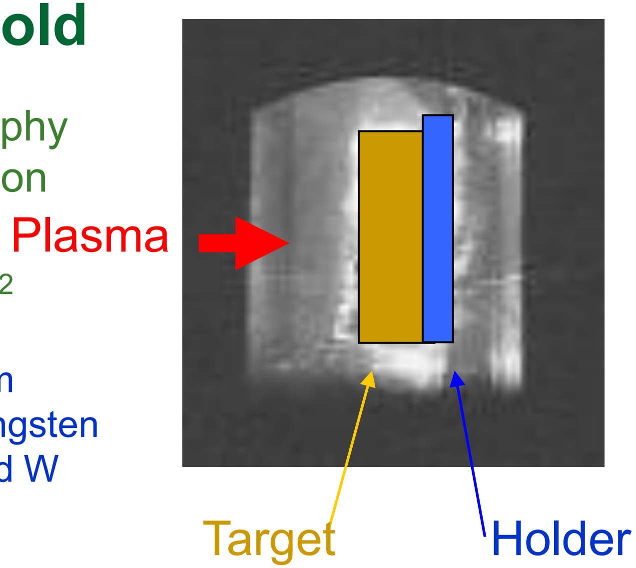

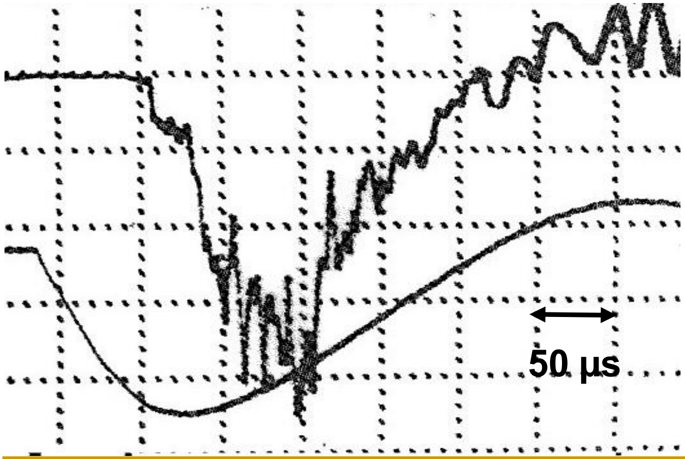

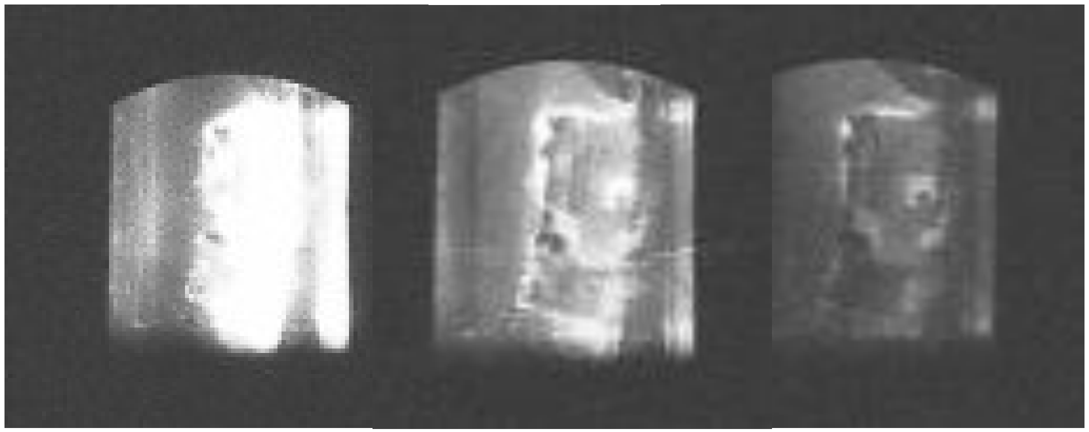

The influence of target atomic mass on the shield dynamics

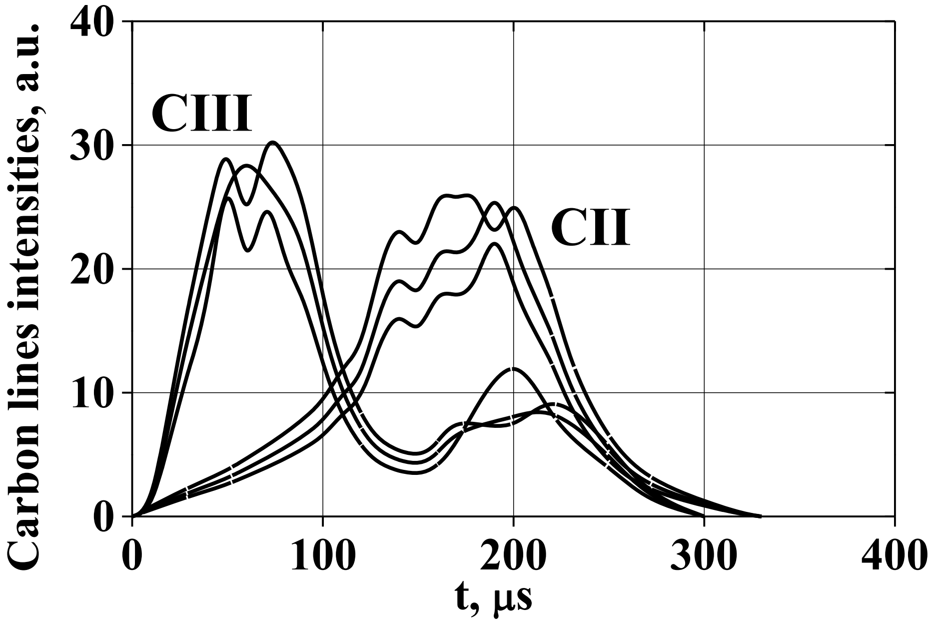

Temporal behavior of CII (2512 Å) and CIII (2296 Å) lines in plasma shield near the surface of the graphite target.

First peak of CIII luminosity (t~50 μs) is caused by the appearance of vapor shield and thermalization of kinetic energy of impacting plasma stream near the target surface.

The shielding layer thickness is increased during the pulse and the temperature value is decreased due to the plasma shield expansion that leads to increase of CII line intensity.

Disruption simulation

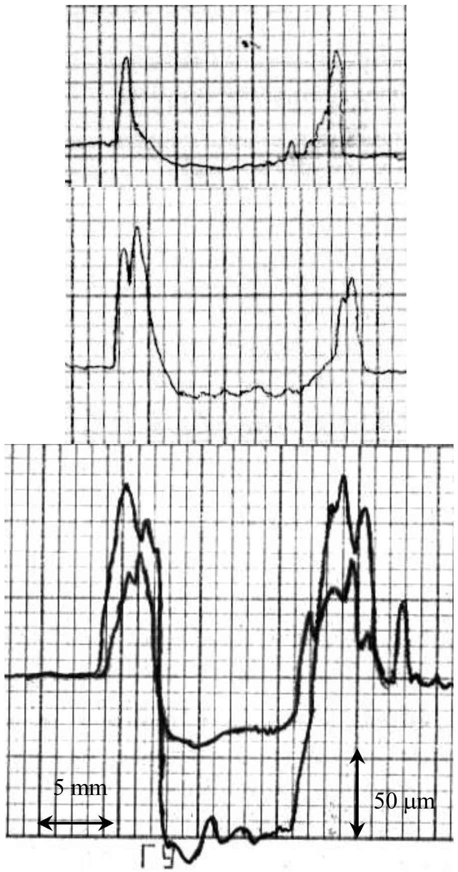

Profiles for Ti target exposed with 1, 3, 5 and 20 pulses. Hole diameter is 1 cm.

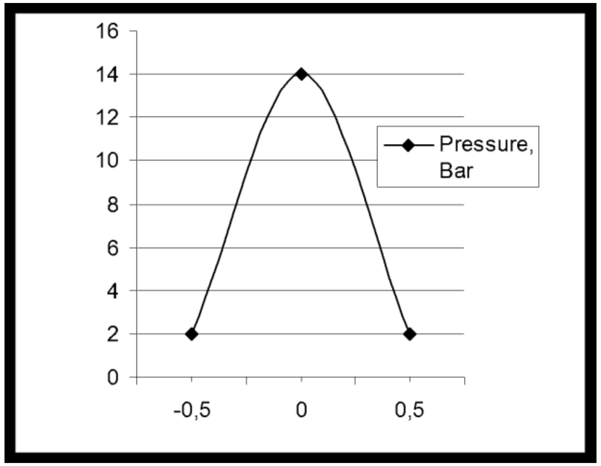

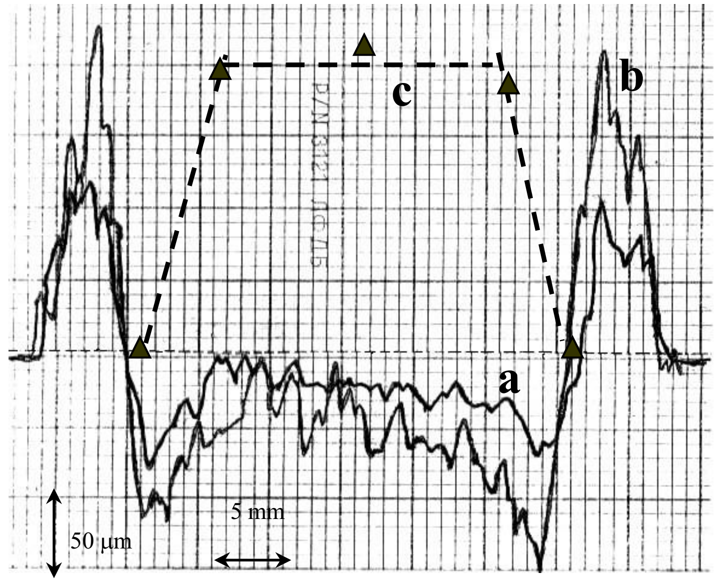

Melt layer profiles for titanium target irradiated with 10 pulses (a) and with 20 pulses (b), with overlay of plasma pressure profile (c). Vertical scale for pressure is 3.5 Bar/div. Hole diameter is 3 cm

The most pronounced melt motion is registered in the region of maximum gradient of plasma pressure

Inclined Exposure:

Melt layer profiles in 2 mutually perpendicular directions for Ti target exposed with 10 pulses

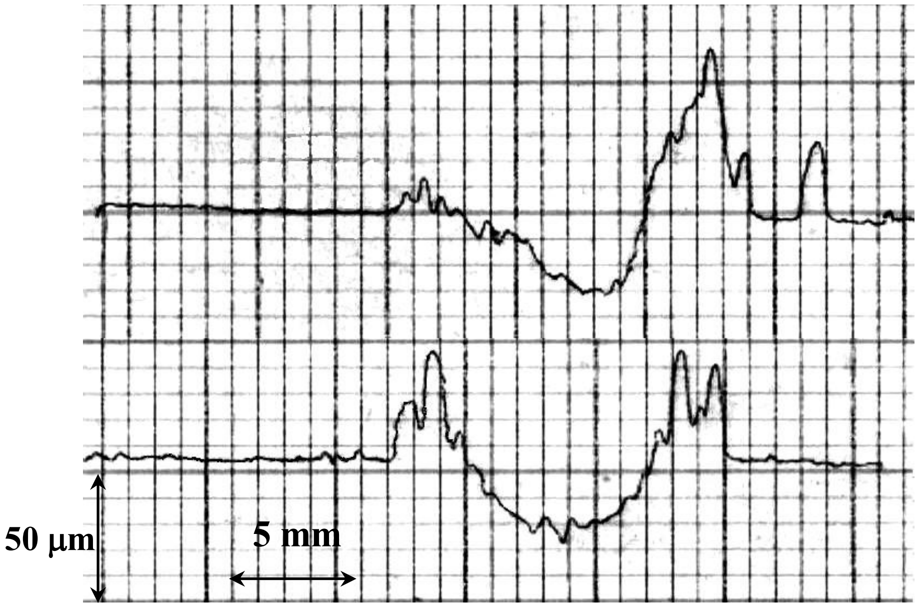

- direction of inclination

- perpendicular direction.

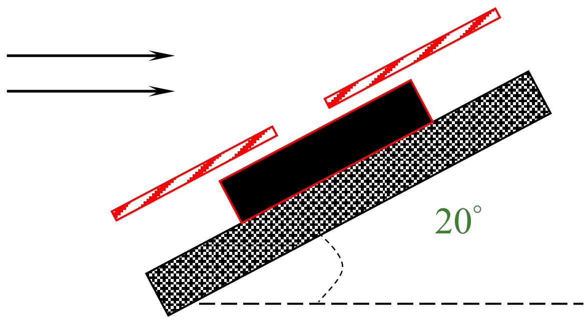

NATIONAL SCIENCE CENTER "KHARKOV INSTITUTE OF PHYSICS AND TECHNOLOGY"

INSTITUTE OF PLASMA PHYSICS

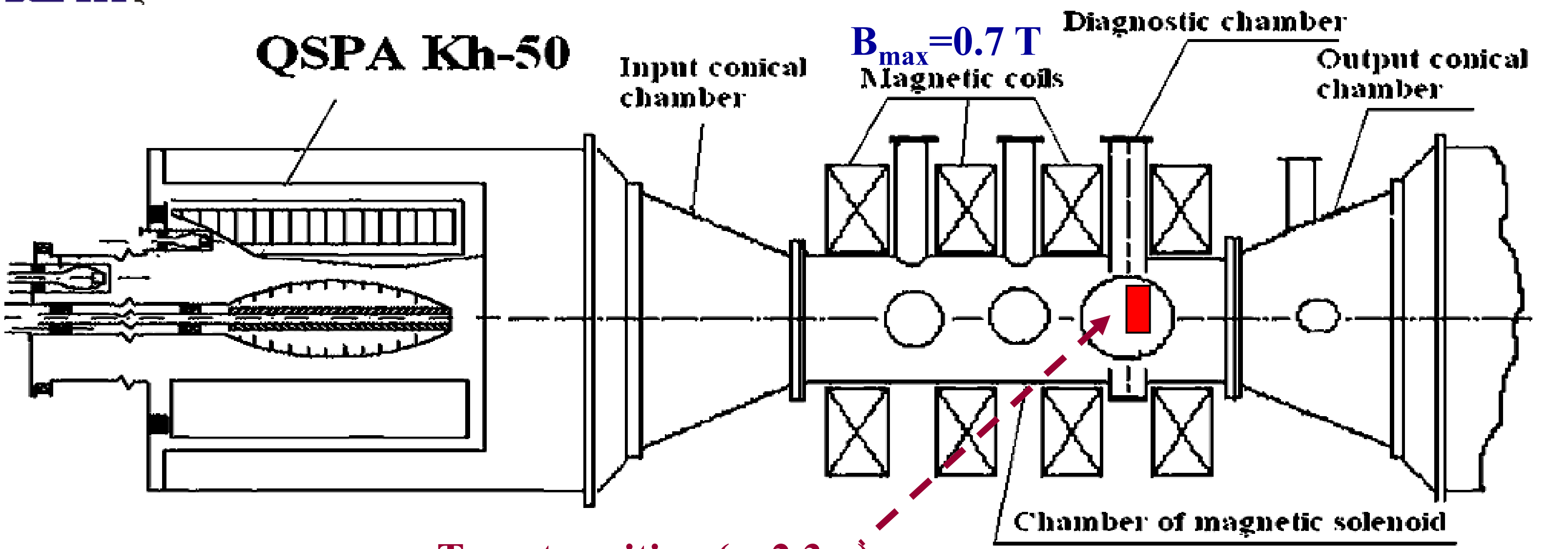

Exposures of tungsten in ELM simulation regimes at QSPA Kh-50

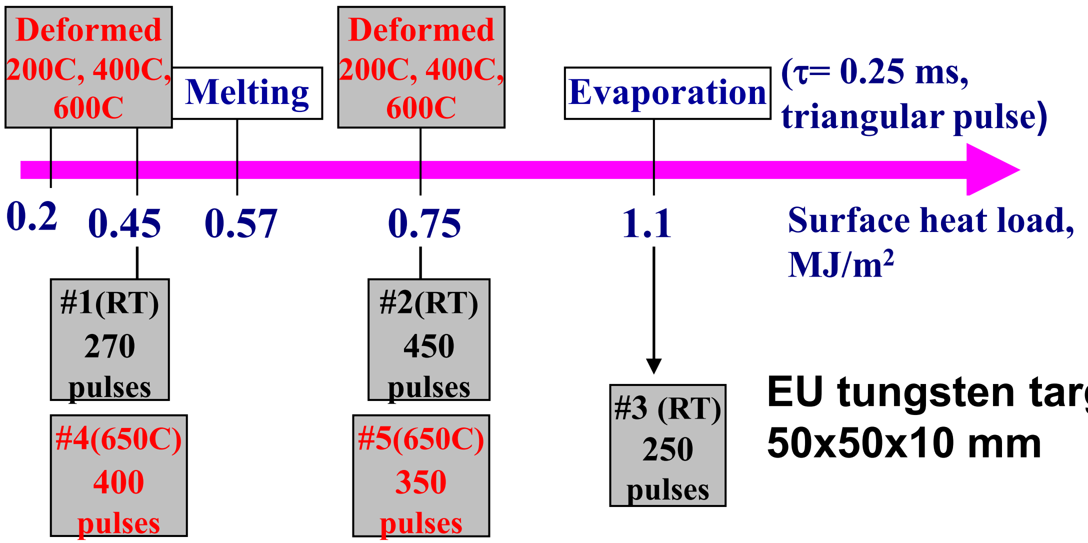

EU tungsten targets 50x50x10 mm

E_i ~ 0.4-0.6 keV,
P_{max}= 3.2 bar; $P_{average}$~1.6 bar
n = (2-5) 10^{15} cm^{-3}
Stream diameter 18 cm.
Pulse duration 0.25 ms
Q_1=0.45 MJ/m²; Q_2=0.75 MJ/m²; Q_3=1.1 MJ/m²;

Heat load to the target surface (“weak” shielding for ELM-like loads)

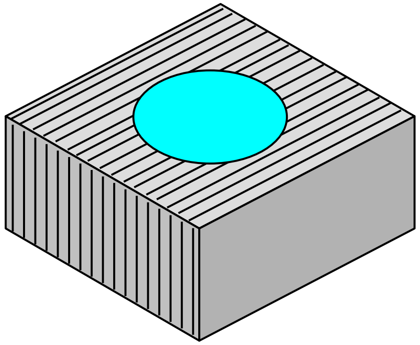

Combined target (FZJ)
Tungsten+CFC

tungsten-graphite target of the same size was prepared in Kharkov
W+C (MPG-7 graphite)

I. Garkusha et al. “Features of plasma energy transfer…” Journ. Nucl. Mater. 2009

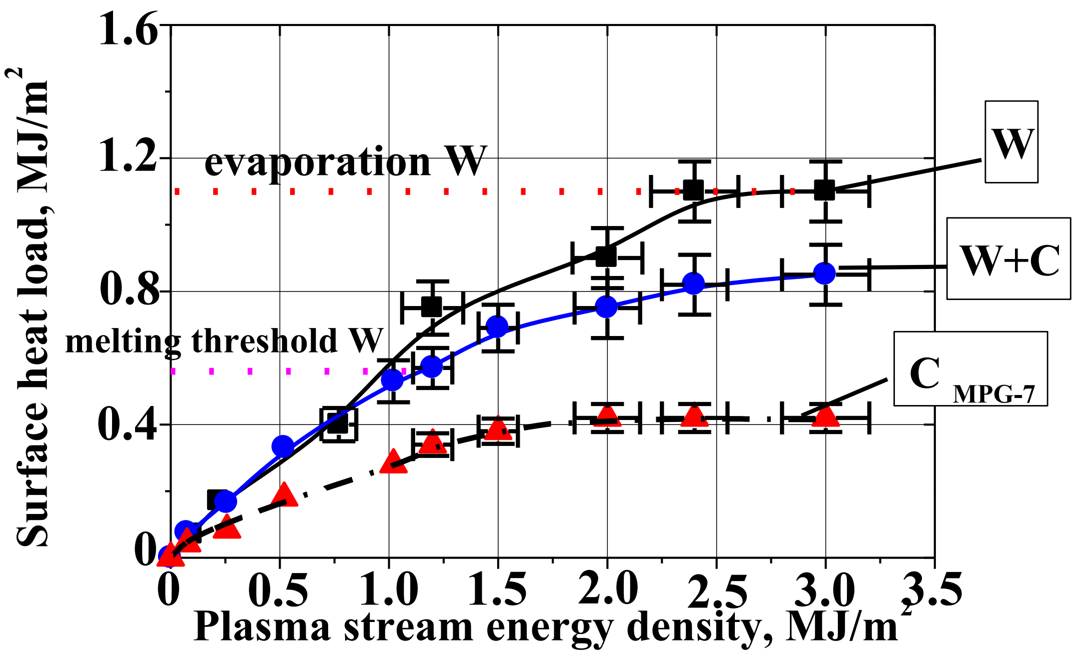

W: vapor shield starts at surface load of 1.1 MJ\m^2
W+C : Carbon shield protects tungsten from evaporation
Clear influence of C evaporation 0.6 MJ\m^2
C: starts to evaporate at 0.42-0.45 MJ/ m^2

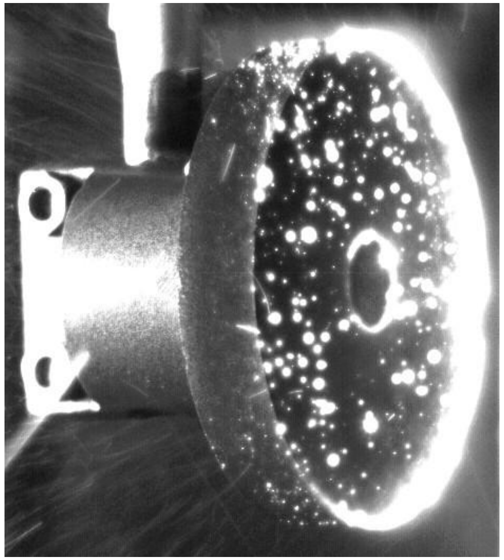

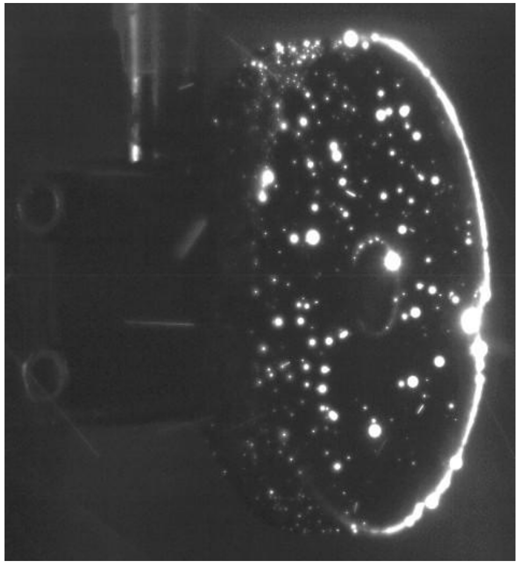

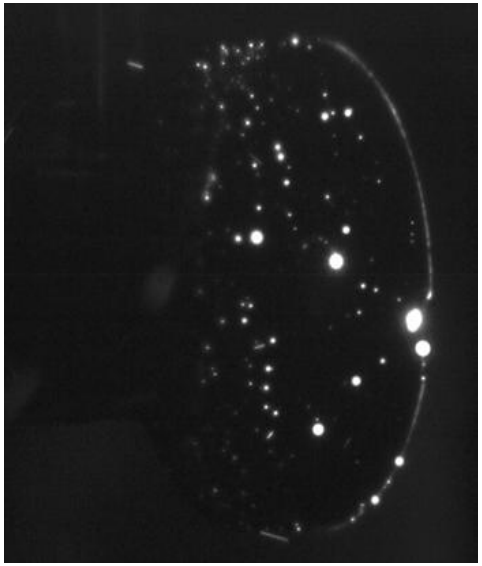

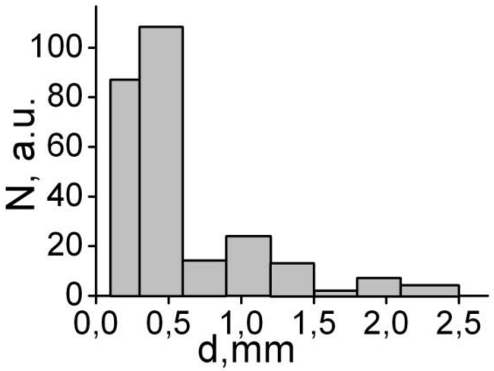

Combined W-C target,
inclined impact 45^0,
t_1=0.95 ms, t_2=1.95 ms,
t_3= 4 ms, τ_{exp} = 0.5 ms,
Q_{surf}=0. 5 MJ/m^2

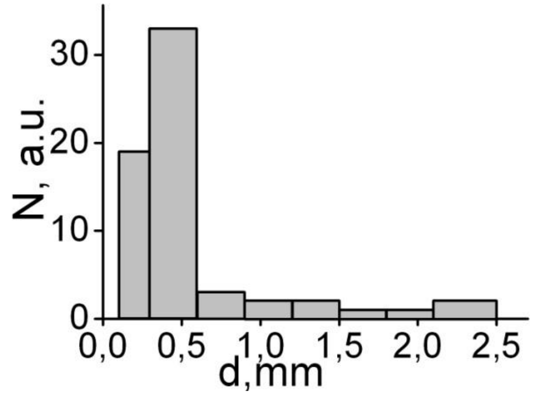

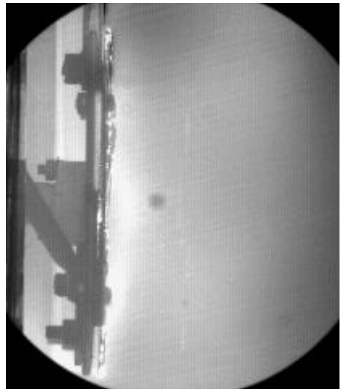

Droplets splashing from melt pool of W target

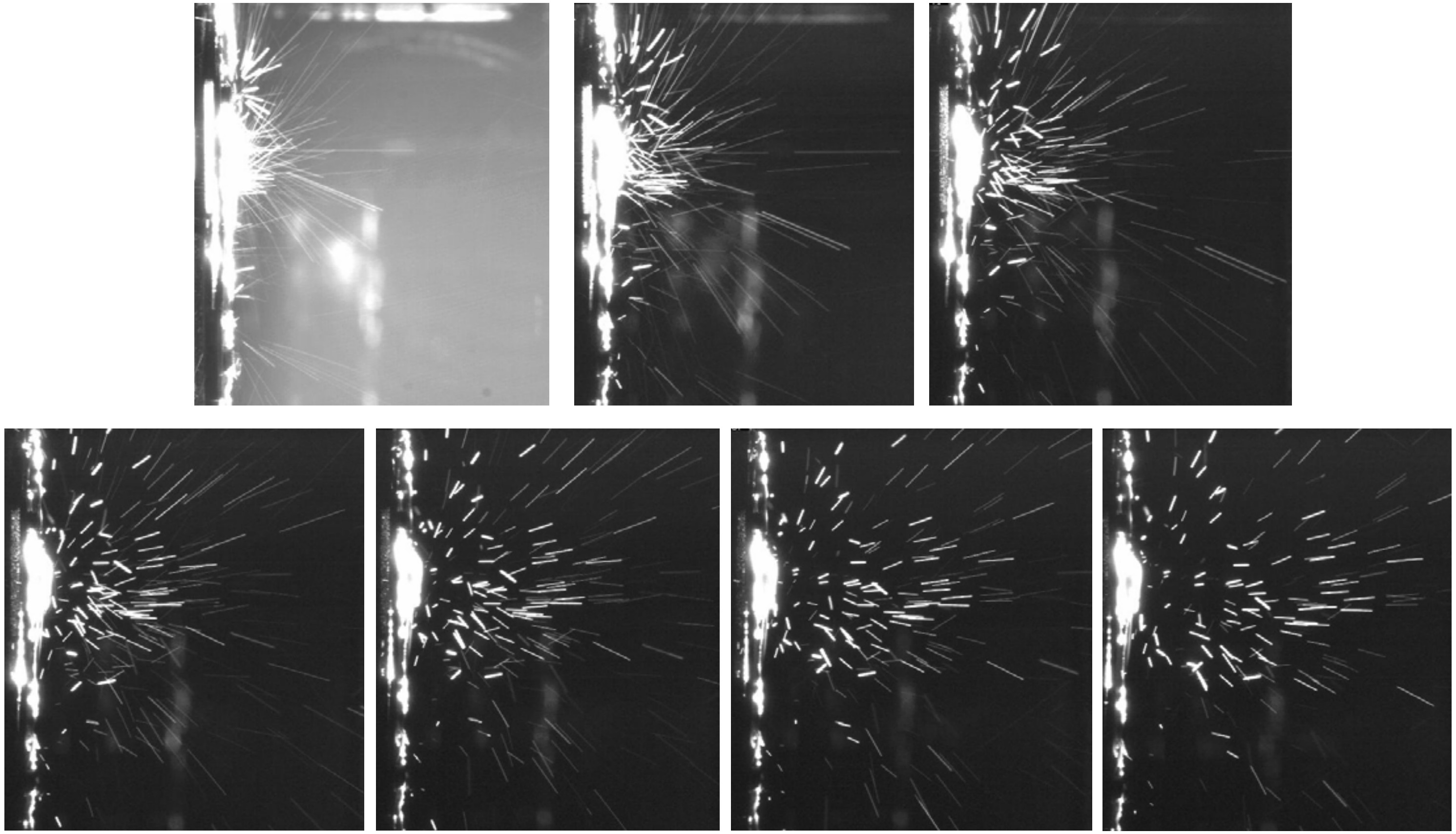

t_1=2.0 ms, τ_{exp}= 1,2 ms

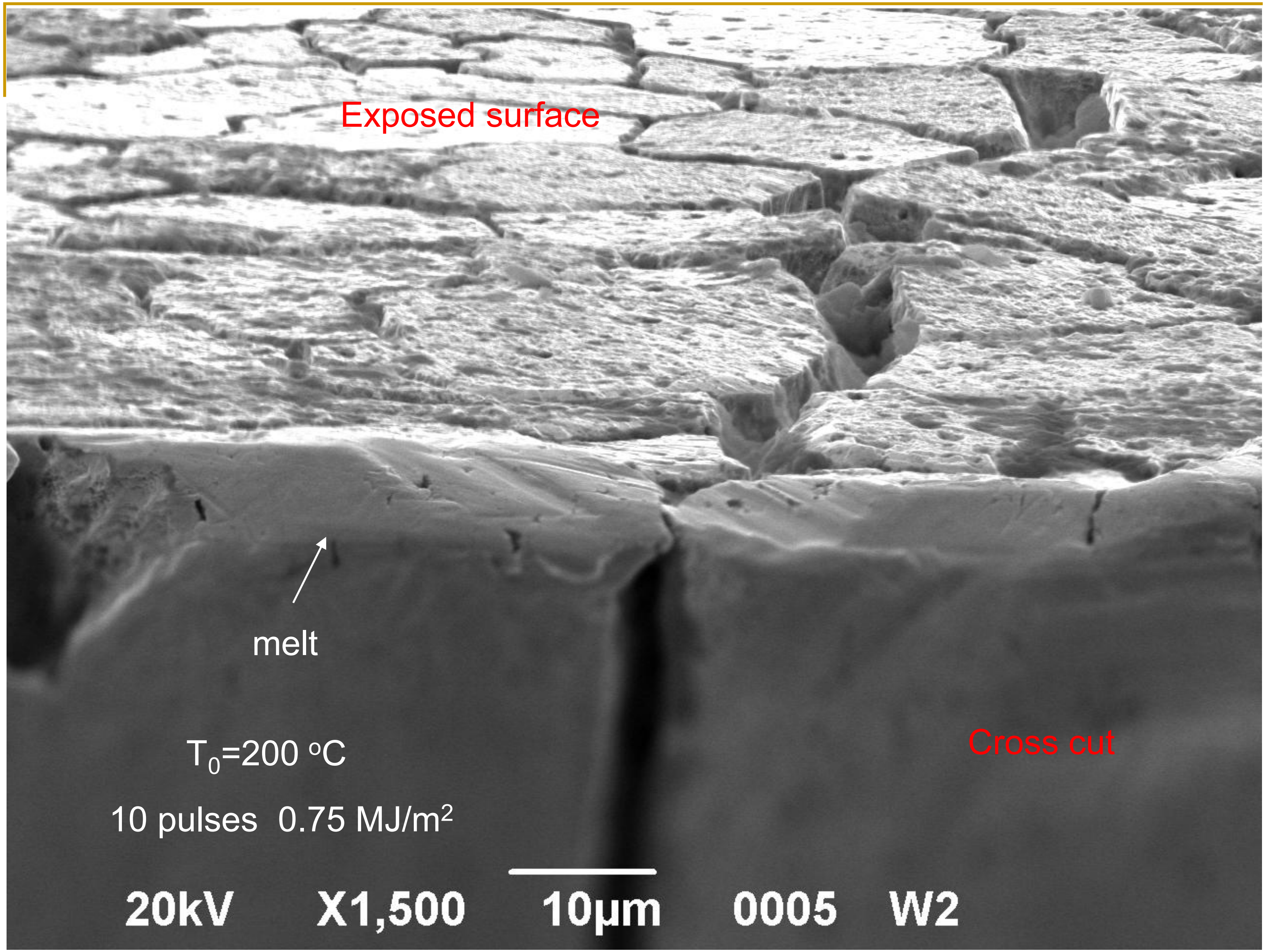
Exposed surface
melt
Cross cut
T_0=200 °C
10 pulses 0.75 MJ/m^2
20kV X1,500 10µm 0005 W2

Tungsten exposures with multiple pulses resulting in melting

Dust issues are extremely important for ITER!

Nano-balls in the crack void after 310 pulses

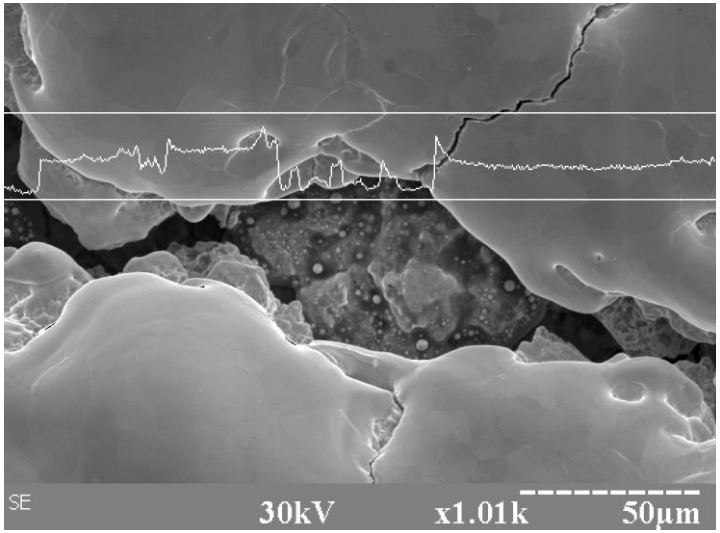

Nano-balls inside the blister after 100 pulses

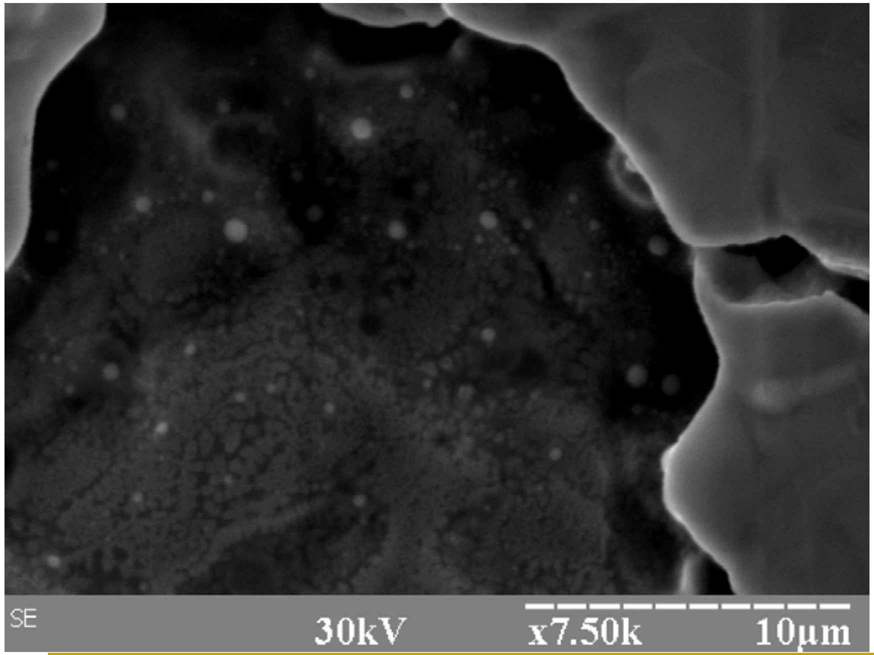

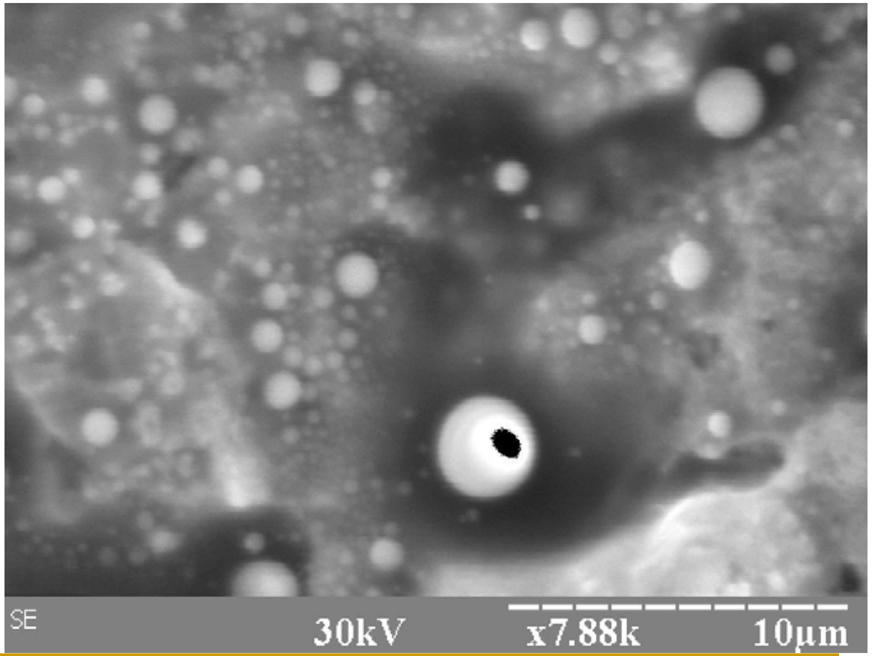

Tungsten exposures with multiple pulses resulting in melting

Threshold changes in surface morphology correlate with profile measurements

Swelling of exposed surface starts after 200 pulses

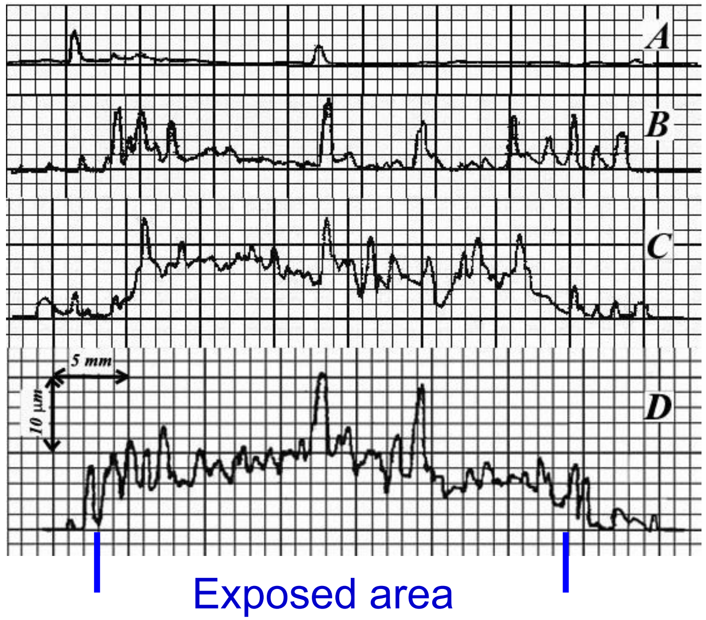

Surface profiles: a- 80 pulses, b- 150 pulses, c- 210 pulses, d- 350 pulses

I. Garkusha et al. “Damage to preheated W…” Journ. Nucl. Mater. 2009

NATIONAL SCIENCE CENTER "KHARKOV INSTITUTE OF PHYSICS AND TECHNOLOGY"

INSTITUTE OF PLASMA PHYSICS

Residual stresses: XRD, $\sin^2\psi$ method

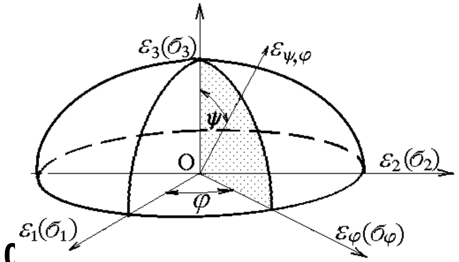

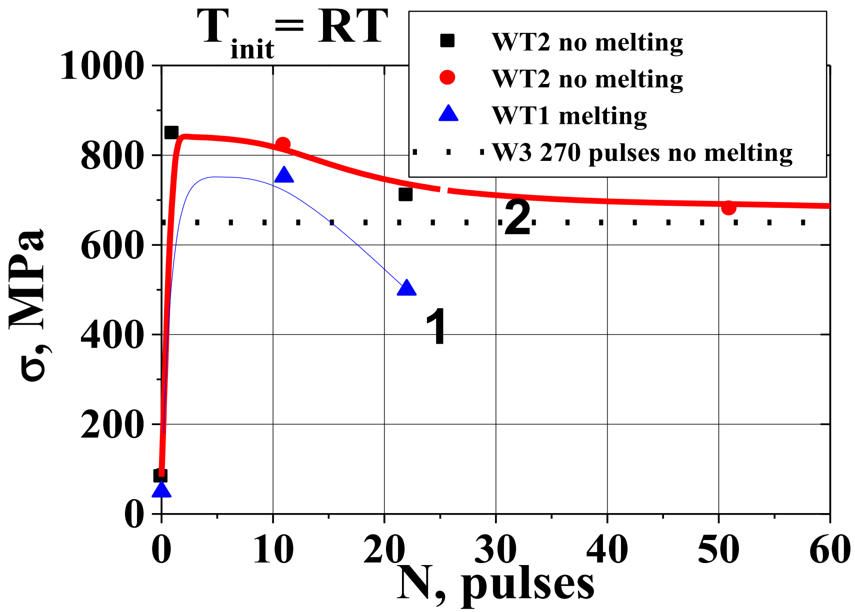

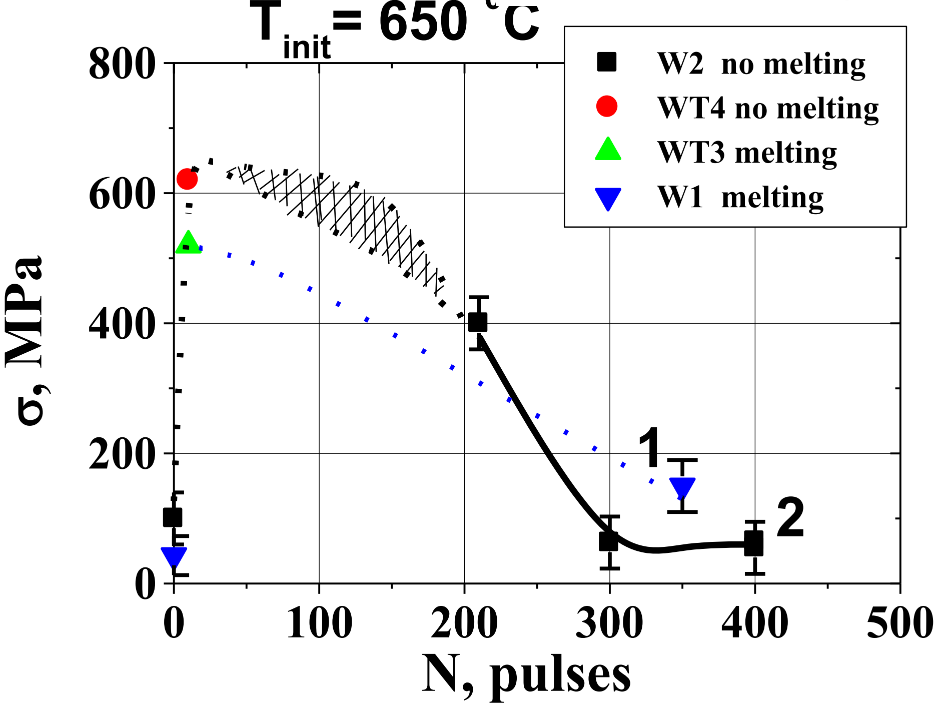

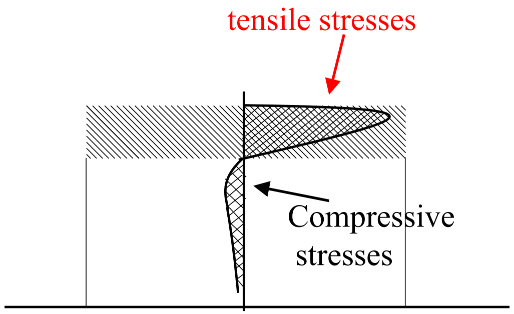

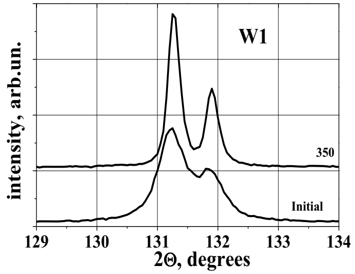

V. Makhlaj et al.“Residual stresses…”Phys.Scr.2009

Tungsten irradiation with repetitive pulses resulting in surface melting

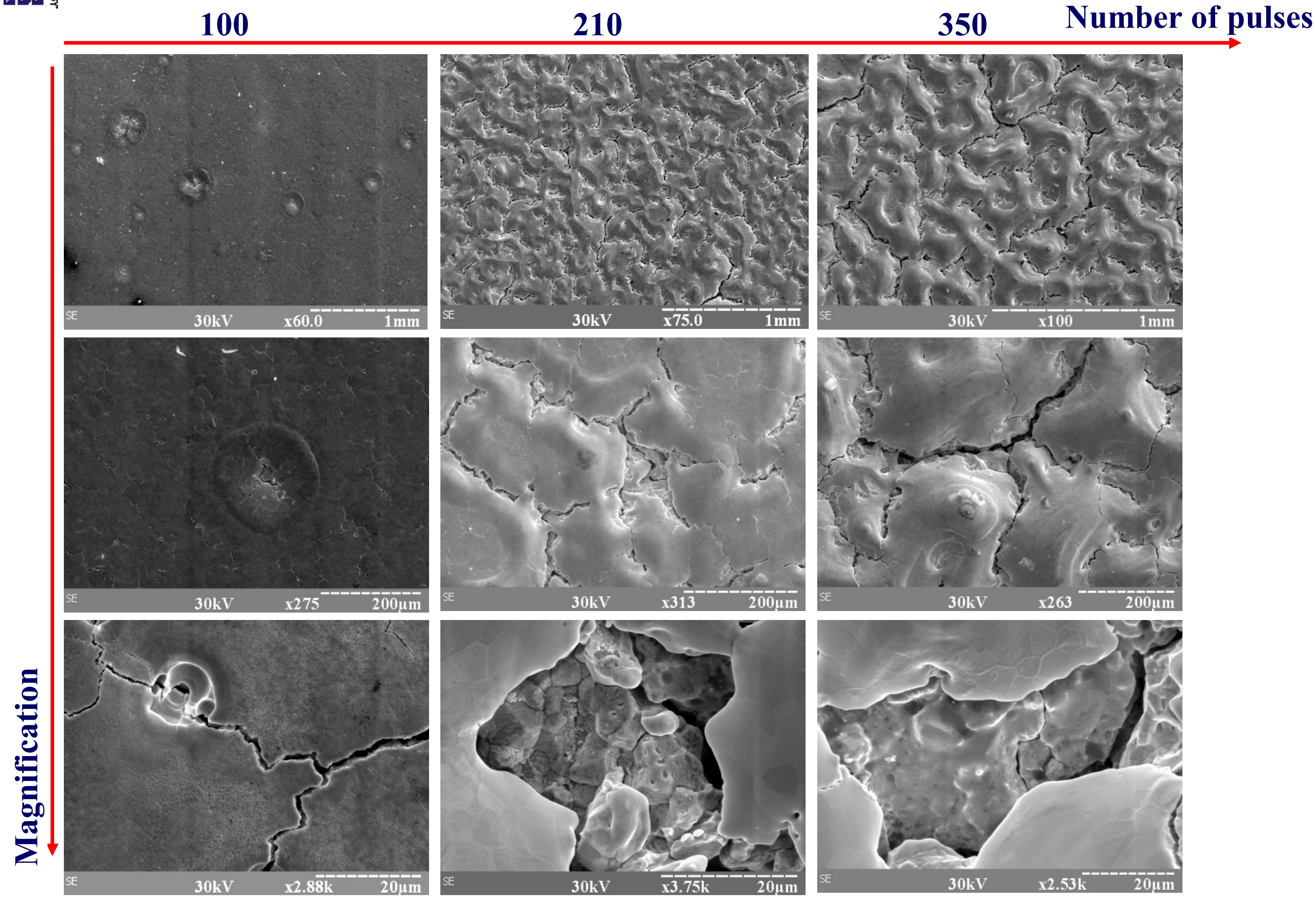

Tungsten irradiation with repetitive pulses resulting in surface melting

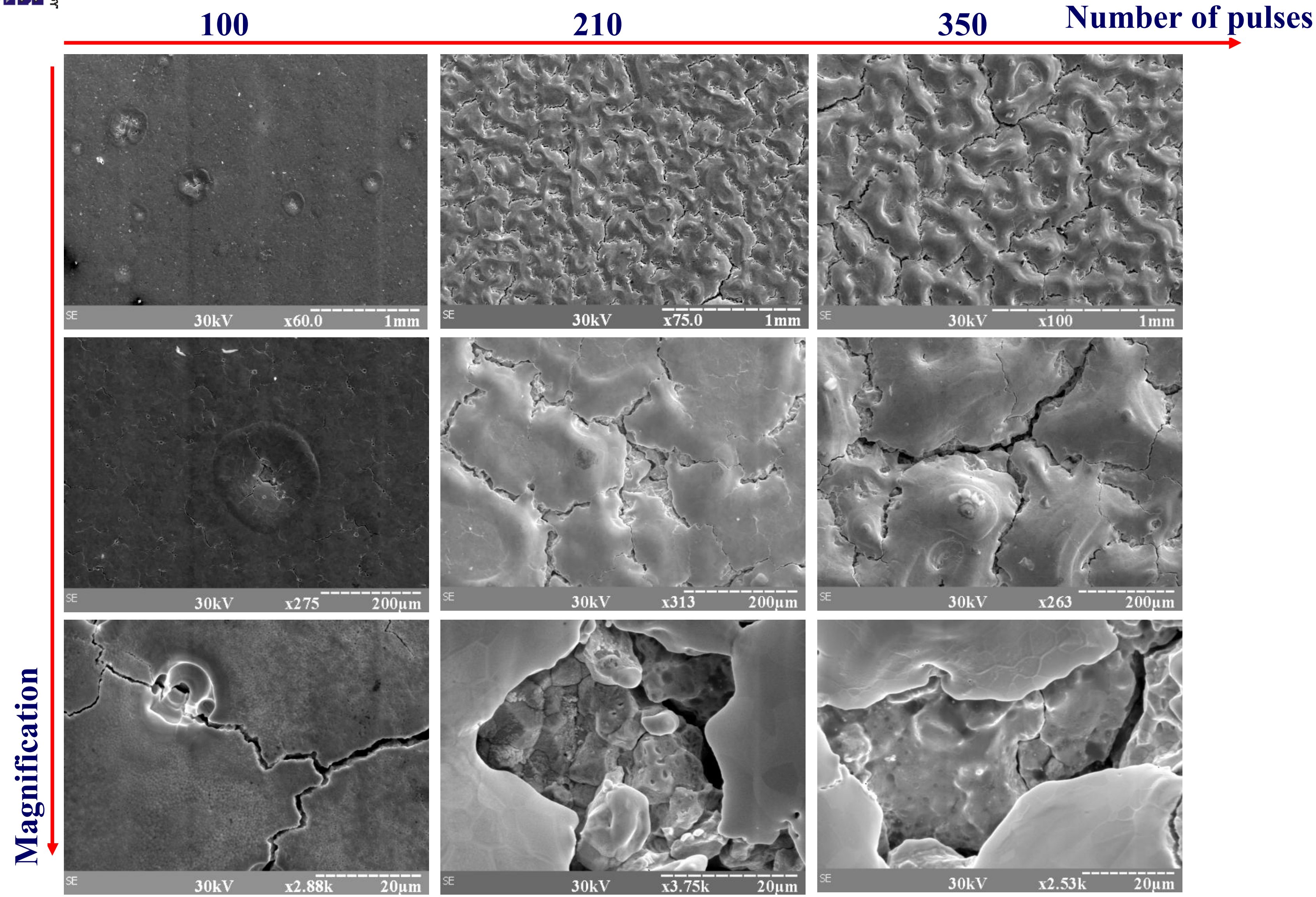

Tungsten irradiation with repetitive pulses resulting in surface melting

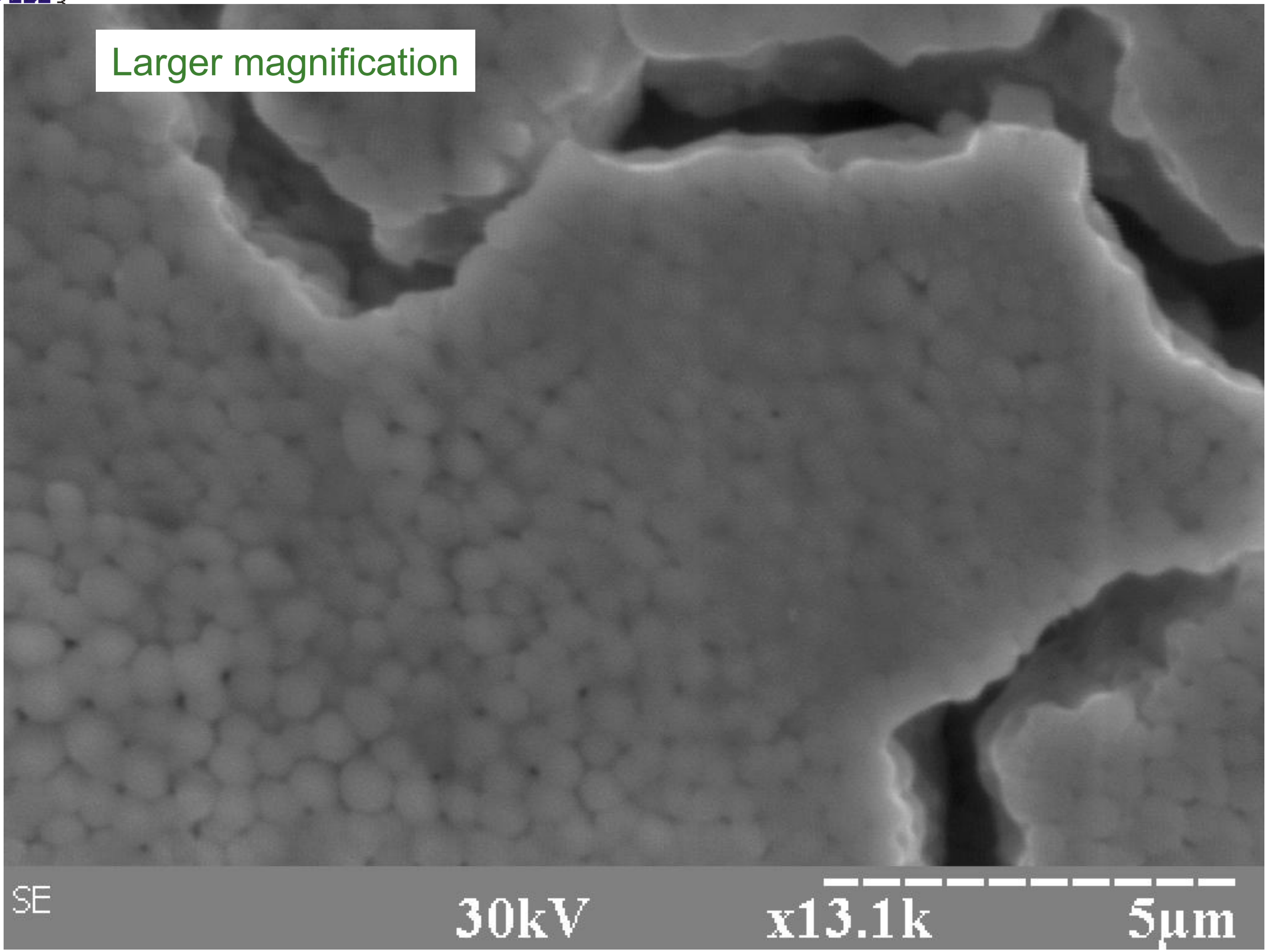

High power plasma streams is unique tool for surface modification

Combination of physical mechanisms:
ion bombardment, heat load (melting, but no evaporation, thermal quenching), shock waves, material alloying with plasma species, mixing in molten stage…………

Microhardness changes induced by pulsed plasma processing

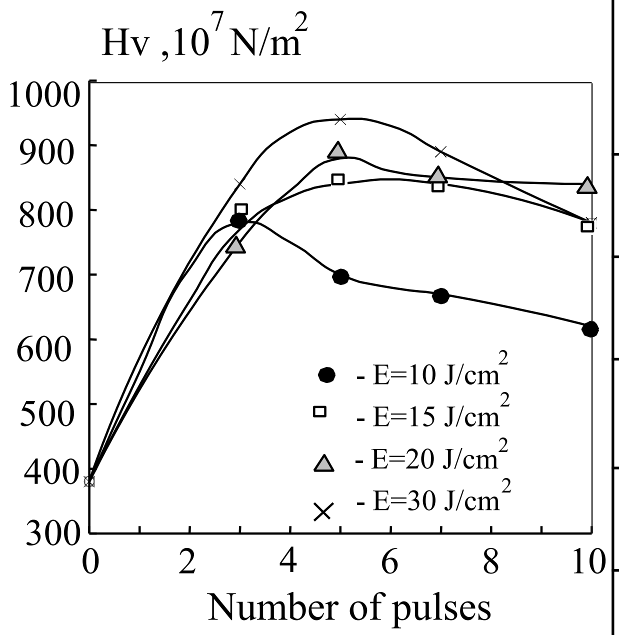

material	H_v, initial	H_v, proc	material	H_v, initial	H_v, proc
steel 10	200	510	65G	350	560
steel 45	250	628	12HN3A	236	630
steel 45 quenched*	370 400	796 870	12HN3A quenched	387	715
40H	252	751	H12	312	510
40H quenched	386	794	H12 quenched *	439 553	554 593
37CrS4	352	742	ShH15	360	770
SAE 1040	264	527	WCo20	1000	1400

Plasma Technologies

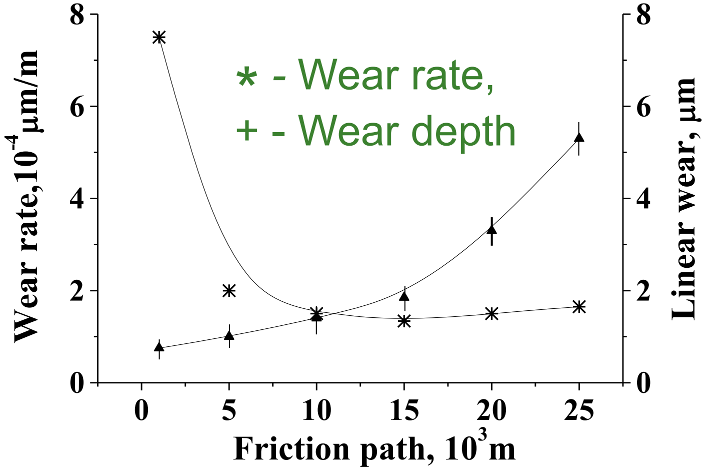

The dynamics of wear for modified surface layers

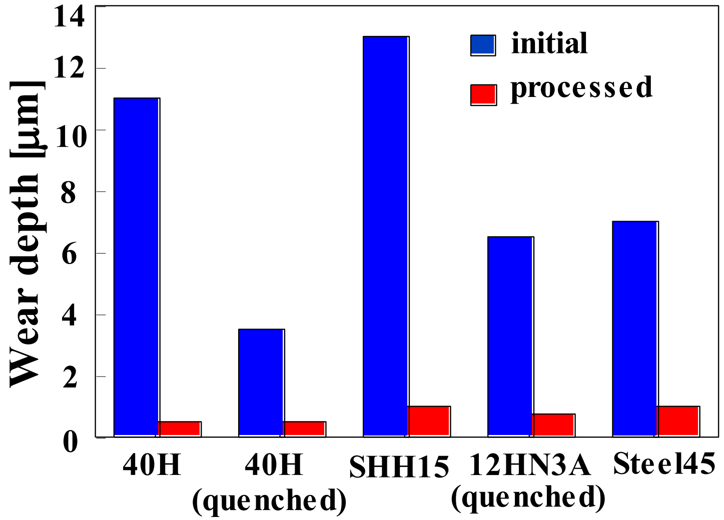

Wear resistance of initial and plasma treated samples (wear path – 1 km)

- **increase of surface wear resistance of structural steels** was measured both for non quenched (**by 10-15 times**) and preliminary quenched (**by 6-8 times**).
- improvement of corrosion properties of structural steels (and also permanent magnets) surfaces was obtained.

Comparative studies with nitrogen, helium, hydrogen plasmas and mixtures show that thermal quenching and nitriding have comparable contribution to the increasing wear resistance

Boron enriched surface layer of steel sample

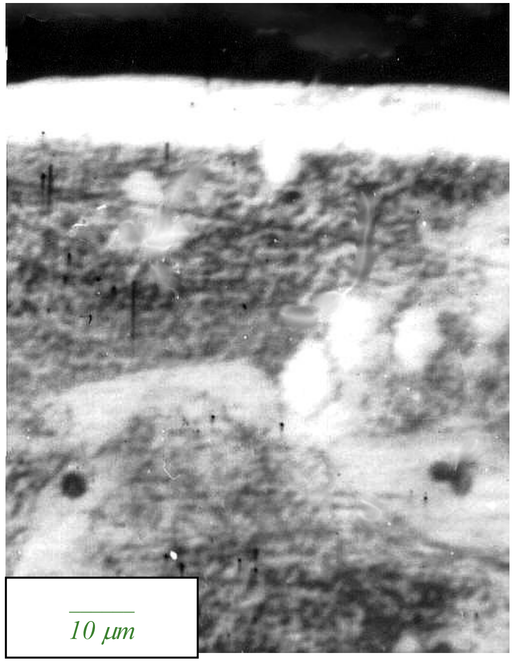

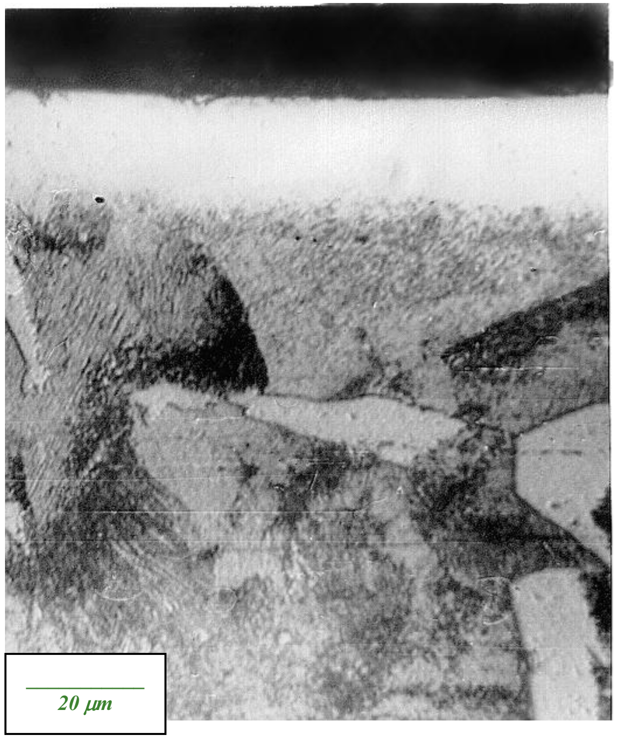

Modification of thick coatings with plasma processing

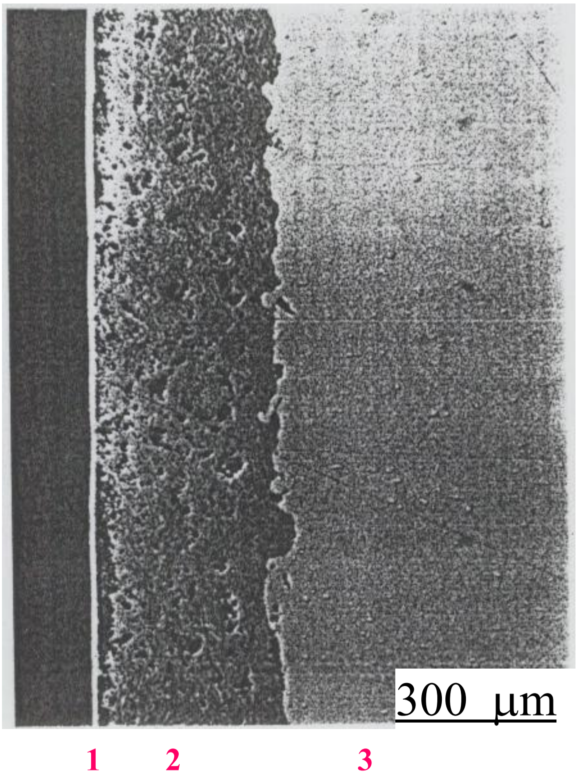

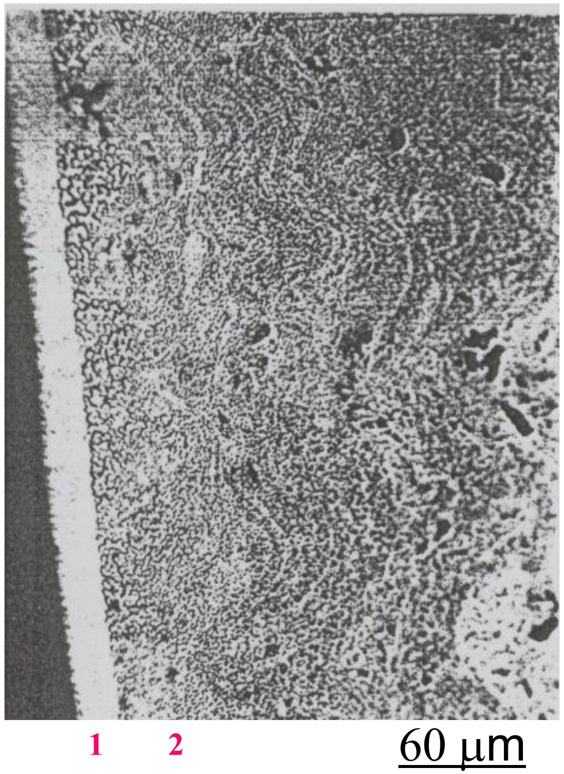

MCrAlY (Co-32Ni-21Cr-8Al-0.5Y w. %), Plasmatechnik AG,Switzerland

Low Pressure Plasma-Sprayed on Inconel 738 substrate

Corrosion resistant upper layer for turbine blades and nozzles, used in combination with thermal barrier coatings

Cr and Al form stable oxides, Y helps

1- modified surface layer, 2- coating, 3-substrate

R_a decreased from 5 μm to *1* μm, ***fine-grained structure resistant to etching, absence of pores***

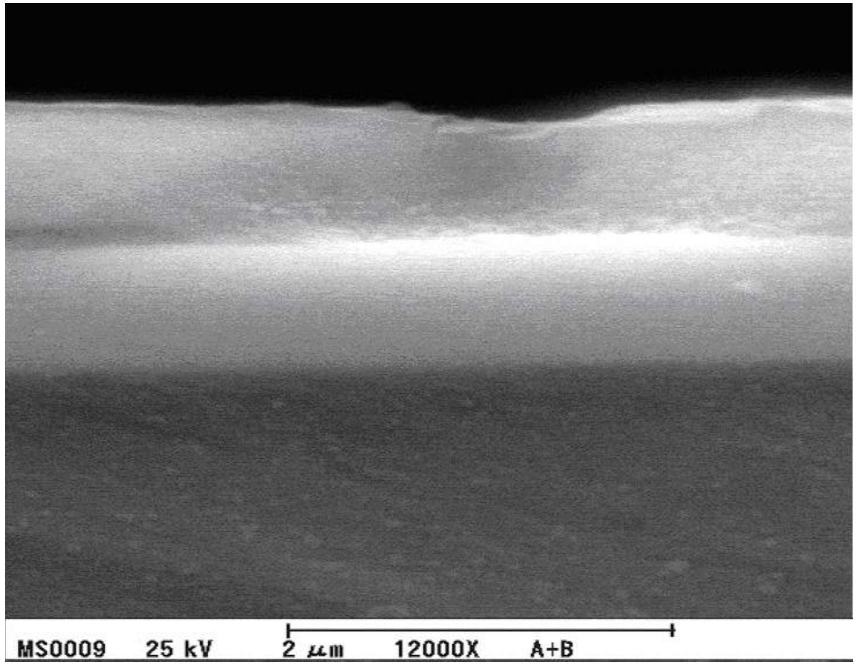

SEM cross-sectional micrograph of tungsten two-layer coating on Cu target

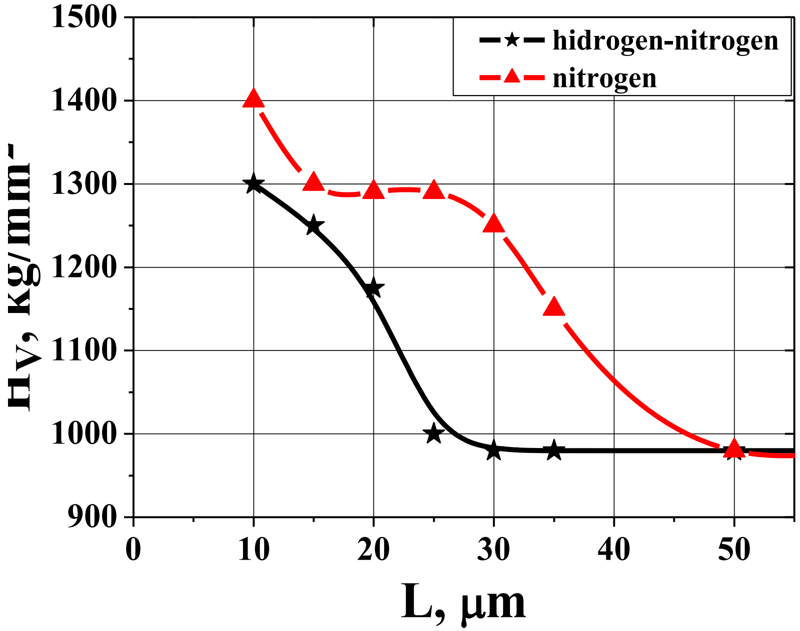

Microhardness depth profiles of WC-20Co samples

V. Makhlai et al. “Material alloying…” Eur. Phys. J. D, 2009

JST MOTORSICH

Some examples

Various turbine blades treated in IPP NSC KIPT

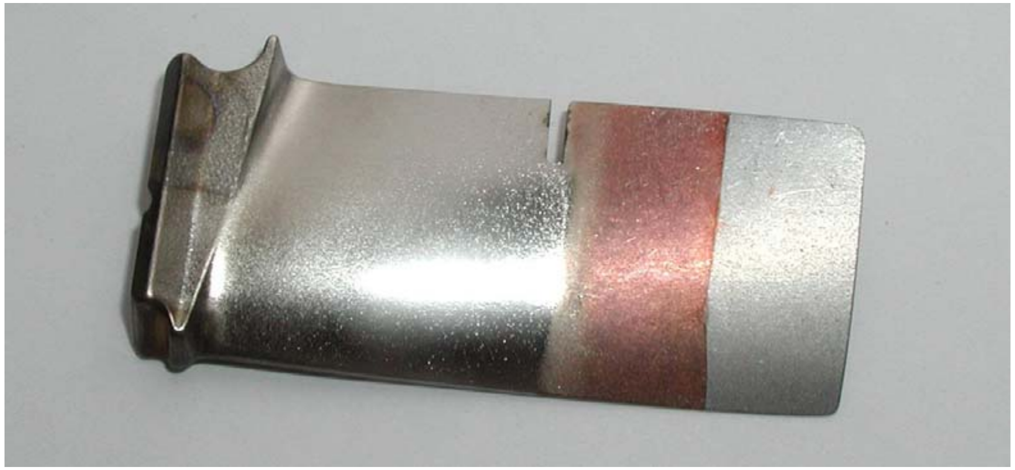

Powerful plasma treatment and coating deposition in different combinations

Thank you
for your attention !

Detectors - AXUV photodiodes

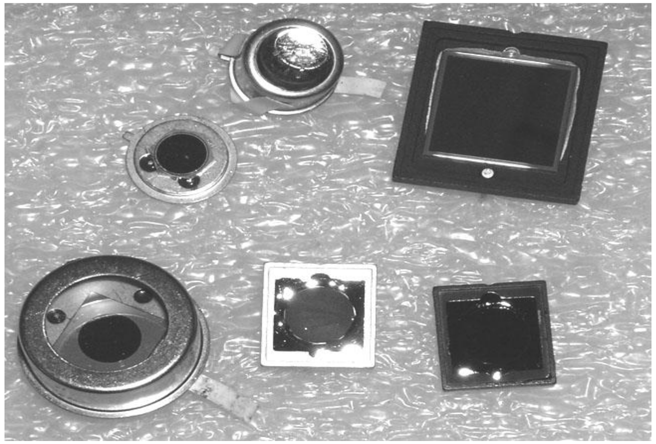

Different types of photodiodes AXUV

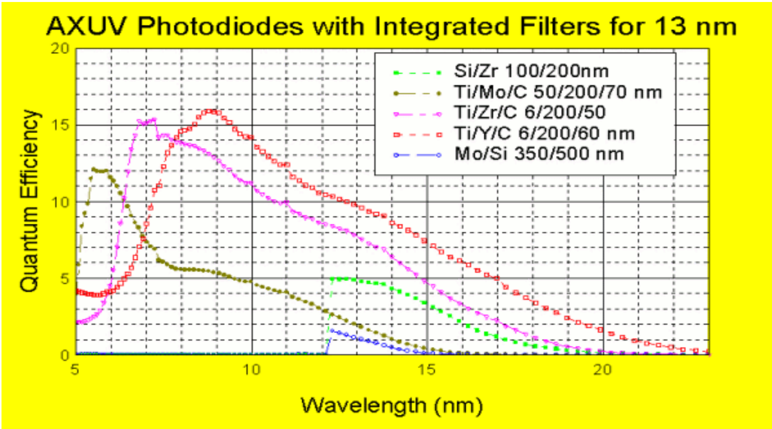

Quantum efficiency of AXUV with integrated filters for different wave-range

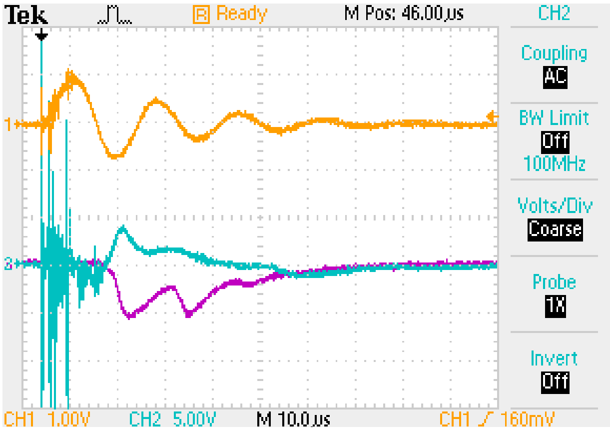

Typical waveform from AXUV diode

PRODUCT NAME	FILTER THICKNESS (nm)	PASS BAND (nm)
AXUV20Ti/Mo/C	70/200/50	5-13
AXUV20Mo/Si	350/500	12.2-15.8
AXUV20Al	300	17-80

Registration of EUV radiation

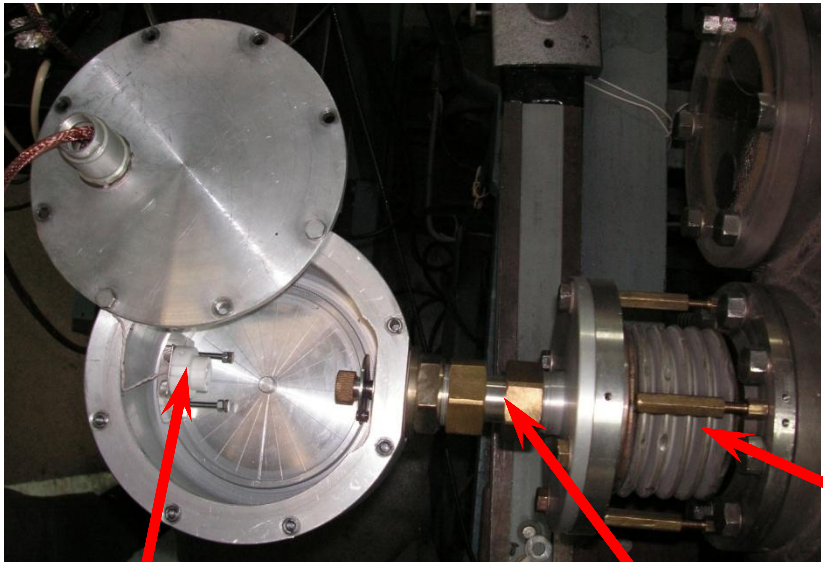

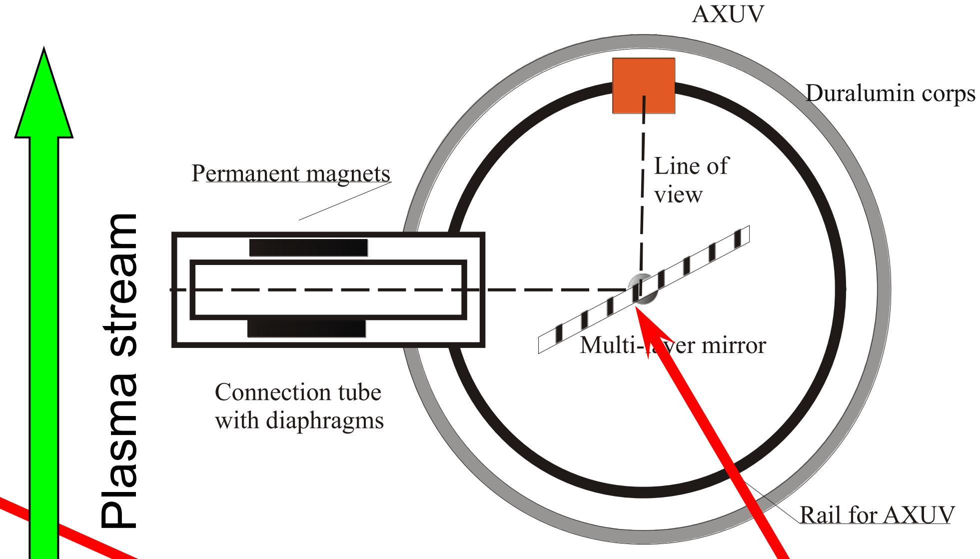

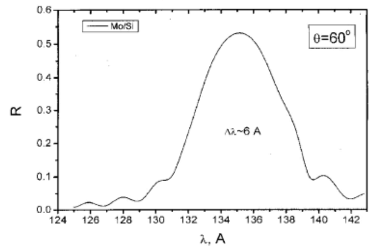

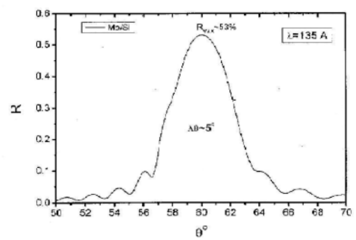

Detectors

AXUV photodiodes – absolute detectors with multilayer thick filter–films for registration different range of wave length

Connection tube

- the inner and outer diaphragms select size of registration zone

- permanent magnets decrease particles influence on detector

Flexible vacuum connection

- Possibility change observation zone in two dimension – z axis and radius of stream

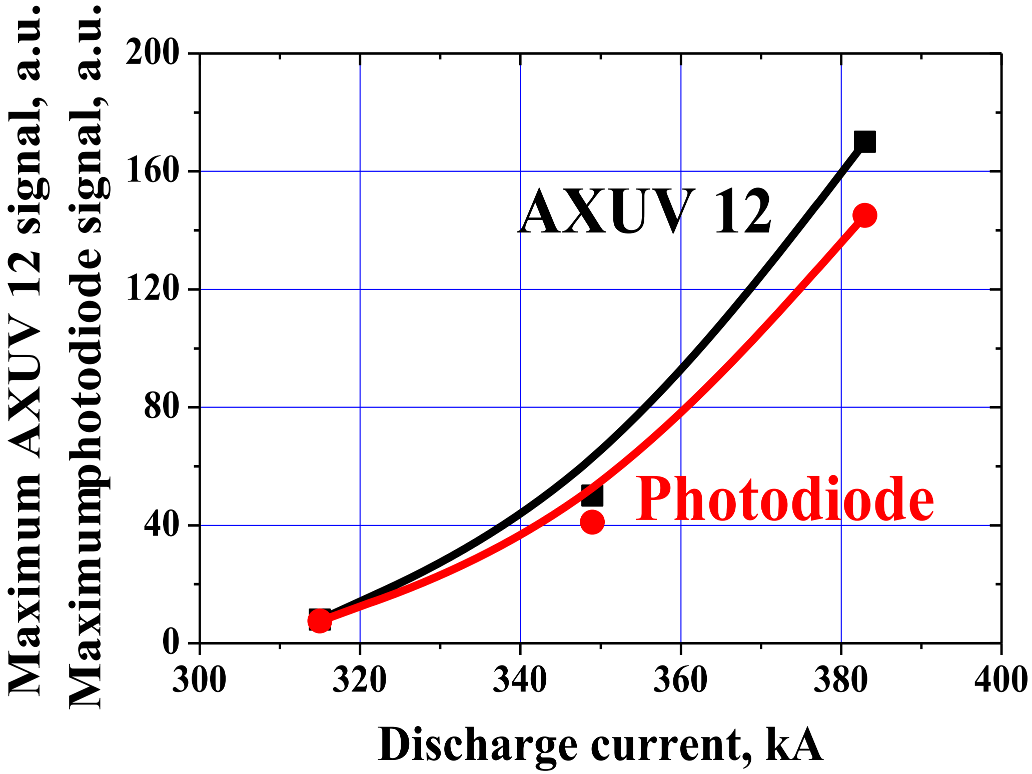

Radiation intensity ~ I_d^2

Energy of UV radiation

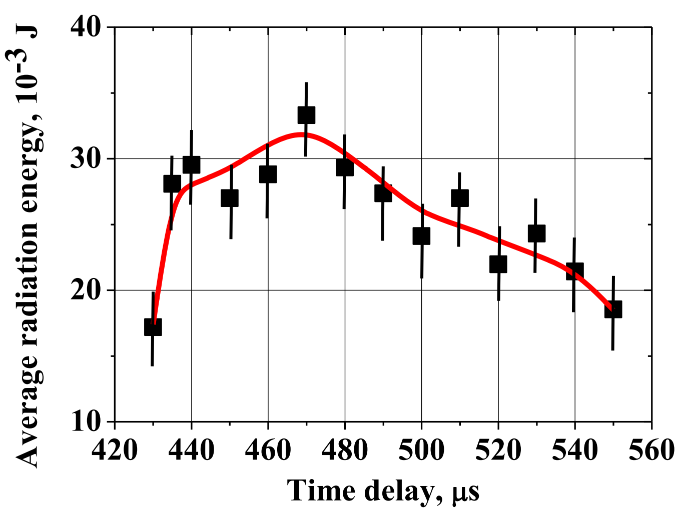

Average radiation energy in wave range 12.2-15.8 nm.
AXUV 20 Mo/Si.

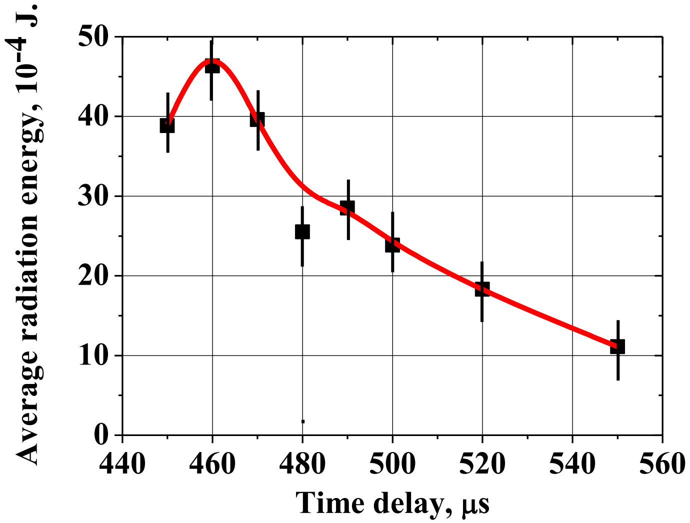

Average radiation energy in wave range 17 - 80 nm.
AXUV 20 Al.

Maximum discharge current 400 kA (Uc= 20 kV), operation with Xenon pulse gas supply (ΔV=10 cm^3). The distance of observation from MPC output is about 6 cm (from anode roads)

NATIONAL SCIENCE CENTER "KHARKOV INSTITUTE OF PHYSICS AND TECHNOLOGY"

INSTITUTE OF PLASMA PHYSICS

Registration of radiation 17-80 nm

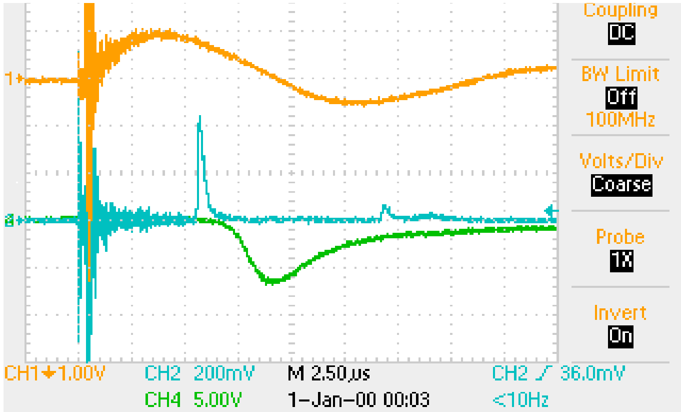

Pure Helium

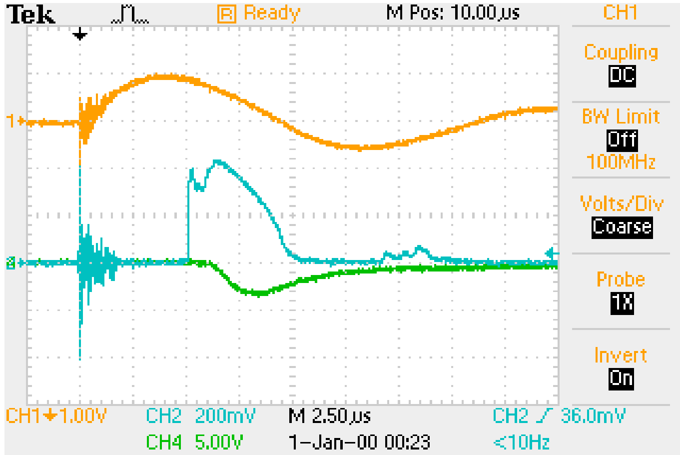

1^{st} pulse He with Xe

P_{He} = 2 Torr

Xe ~ 7 cm^3

(normal conditions)

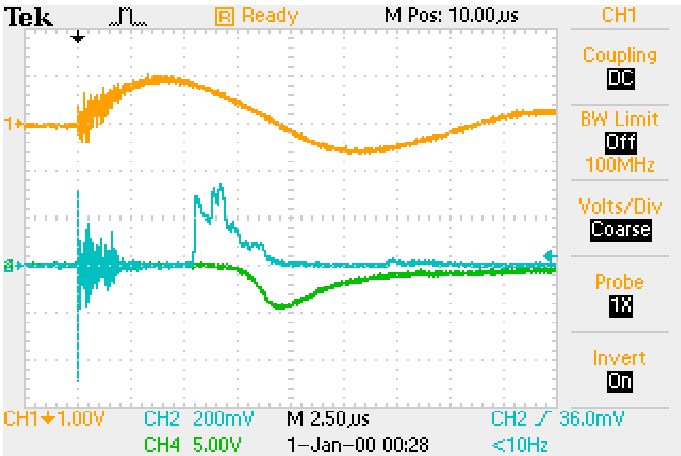

2^{nd} pulse He with Xe

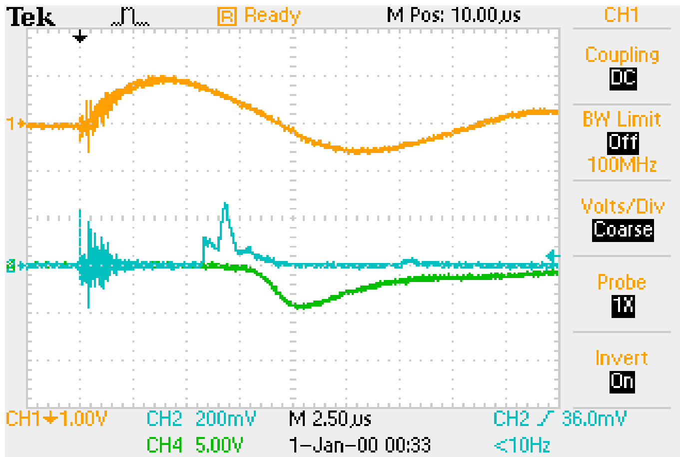

3^{rd} pulse He with Xe

Absorption of EUV radiation by xenon

Cell of Crack Mesh after Different Number of Pulses

(Surface Heat Load - **0.75 MJ/m^2**)

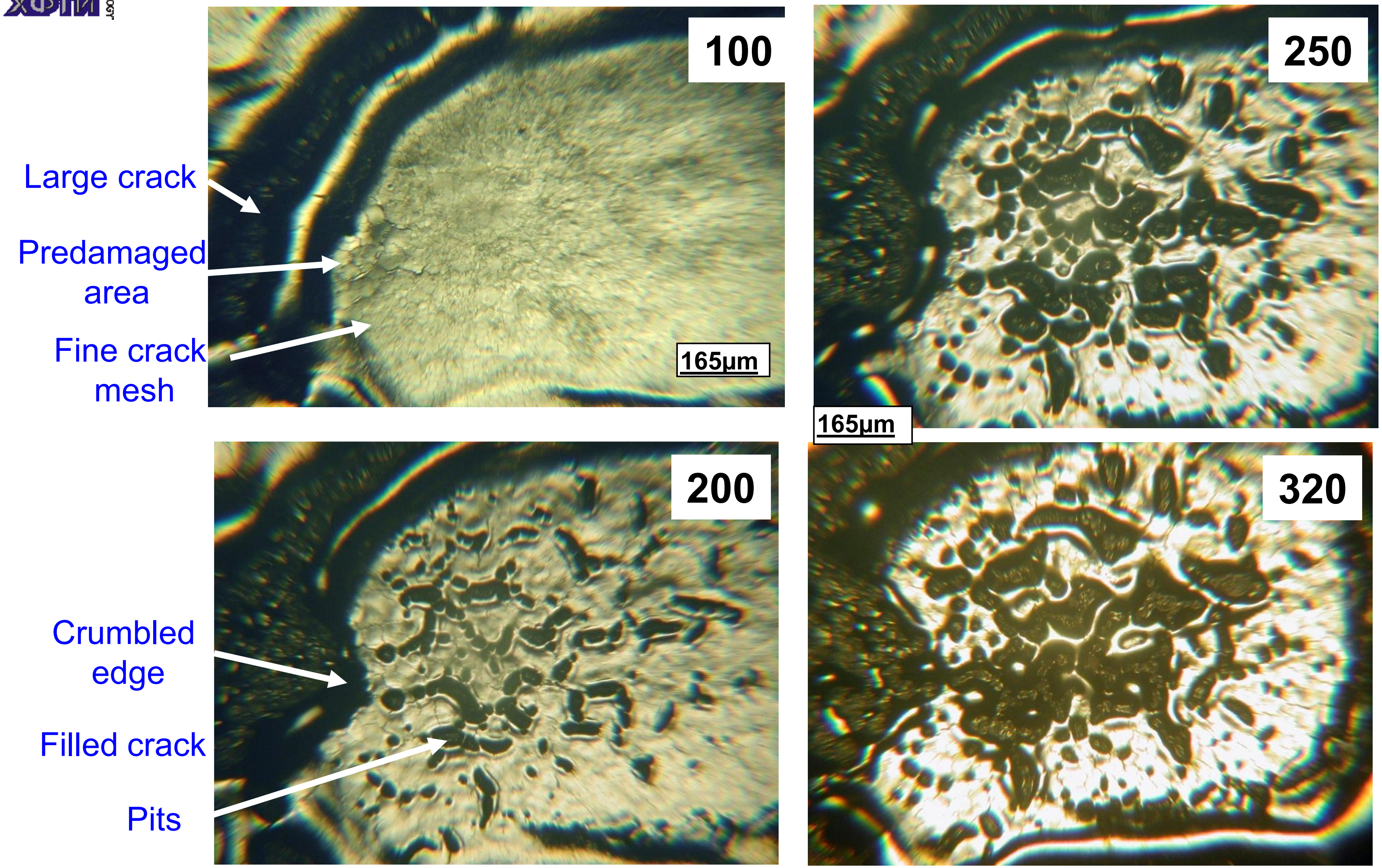

ELM-Like Heat Loads Resulting in Surface Melting

(Surface Heat Load - **0.75 MJ/m^2**)

Fine cracks trigger a qualitative evolution of sample surface after a few hundreds of pulses (corrugation, pits) accompanied by growing mass loss rate.

It is not constant being larger than that of the regime 1: by 2, 3 and 5 times in the course of the first 100, next 100 and next 50 pulses accordingly

Evolution of fine crack mesh

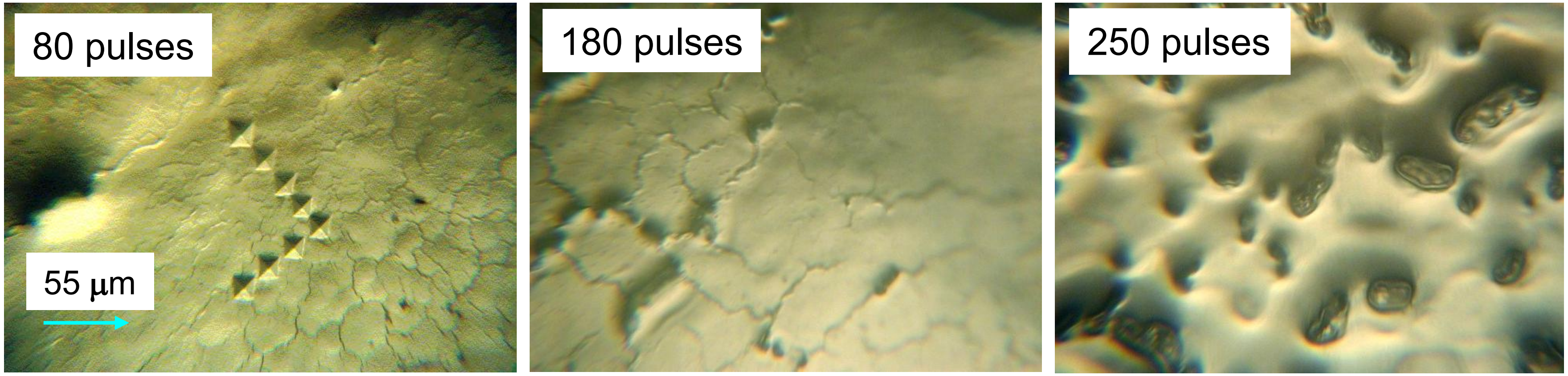

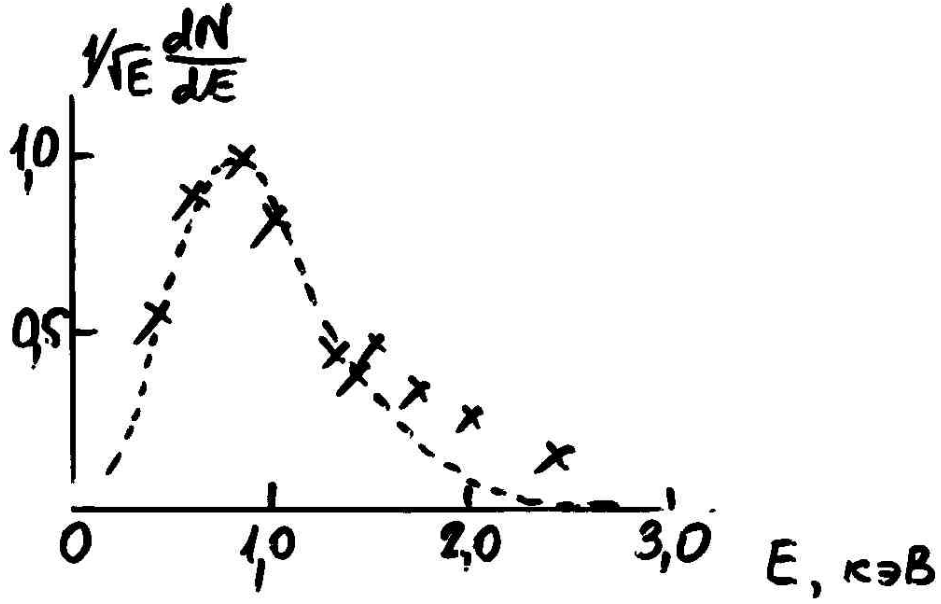
1/√E dN/dE
1,0
0,5
0
1,0
2,0
3,0
E, кэВ

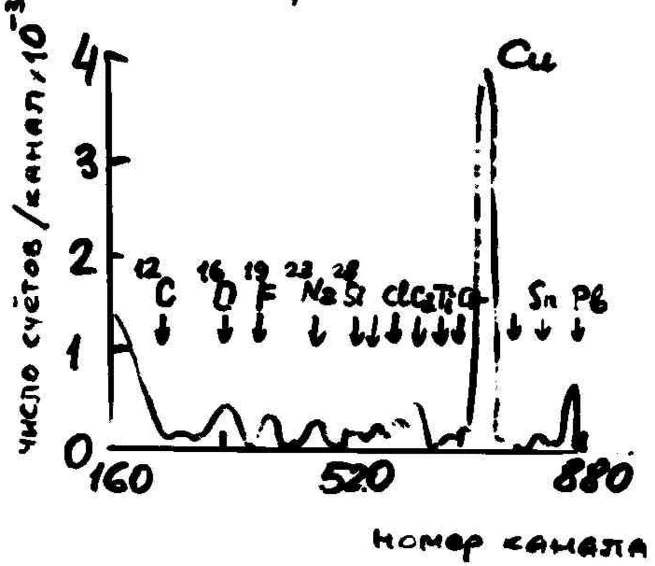
число счётов / канал × 10^3
4
3
2
1
0
160
520
880
Cu
12 C
16 O
19 F
23 Na
28 Si
Sn
Pb
номер канала